N O T I C E

5?1F

NASA

Technical Memorandum 83854

Estimating Ocean-Air Heat Fluxes During Cold Air Outbreaks by Satellite

(NASA-TM-83854) ESTIMATING OCEAN-AIR HEAT FLUXES DURING COLD AIR OUTBREAKS BY SATELLITE (NASA) 52 p HC A04/MF A01 CSCL 04B

N82-19781

Unclas

G3/47 16370

Shu-Hsien Chou and David Atlas

ORIGINAL CONTAINS
COLOR ILLUSTRATIONS

NOVEMBER 1981

National Aeronautics and
Space Administration

Goddard Space Flight Center
Greenbelt, Maryland 20771

TM-83854

ESTIMATING OCEAN-AIR HEAT FLUXES DURING COLD AIR OUTBREAKS BY SATELLITE

Shu-Hsien Chou

and

David Atlas

Goddard Laboratory for Atmospheric Sciences

November 1981

NASA/GODDARD SPACE FLIGHT CENTER
Greenbelt, Maryland 20771

PRECEDING PAGE BLANK NOT FILMED

ABSTRACT

Nomograms of mean column heating due to surface sensible and latent heat fluxes have been developed from Stage and Businger's (1981a, b) boundary layer model for cold air outbreaks over warm water. Mean sensible heating of the cloud free region is related to the cloud free path (CFP, the distance from the shore to the first cloud formation) and the difference between land air and sea surface temperatures, θ_1 and θ_0, respectively. Mean latent heating is related to the CFP and the difference between land air and sea surface specific humidities, q_1 and q_0, respectively. Results are also applicable to any path within the cloud free region. Corresponding heat fluxes may be obtained by multiplying the mean heating by the mean wind speed in the boundary layer. The sensible heating estimated by the present method is found to be in good agreement with that computed from the bulk transfer formula. The sensitivity of the solutions to the variations in the initial coastal soundings and large scale subsidence is also investigated. The results are not sensitive to divergence but are affected by the inital lapse rate of potential temperature; the greater the stability, the smaller the heating, other things being equal. Unless one knows the lapse rate at the shore, this requires another independent measurement. For this purpose we propose to use the downwind slope of the square of the boundary layer height, the mean value of which is also directly proportional to the mean sensible heating. The height of the boundary layer should be measurable by future spaceborne lidar systems. The general behavior of the mean sensible heating, the potential temperature and the height of the boundary layer as a function of downwind distance within the cloud free region and their relations to several important parameters are studied analytically in the Appendix. By-products include the finding that the sensible (latent) heat flux is virtually linear with the contrast in land air and sea surface temperature (specific humidities), thus providing a new kind of flux parameterization in lieu of the classical bulk transfer formulas. The applicability of the results to lake-effect snowstorms is also noted. Finally, the method can be used in reverse to check the validity of boundary layer models.

ESTIMATING OCEAN-AIR HEAT FLUXES
DURING COLD AIR OUTBREAKS BY SATELLITE

1. INTRODUCTION

Air-sea interaction plays a very important role in a wide range of weather, climate, and ocean problems. There is increasingly persuasive evidence that anomalies in sea surface temperature (SST) control both regional and global climatic anomalies (e.g., Bjerknes, 1966, 1969; Namias, 1969, 1978). The anomalous SST obviously affects the atmospheric circulation through the ocean-air heat fluxes. For this reason much effort is going into the accurate parameterization of the fluxes of heat, moisture, and momentum in GCM models. The ocean to air heat fluxes are also related to the prevailing synoptic pattern and mesoscale convective system (Kung and Siegal, 1979; Sheu and Agee, 1977; Warsh, 1973). These fluxes over the warm water of the Kuroshio current and the Gulf stream are generally known to have profound effects on cyclogenesis and storm intensification, particularly on the development of the wintertime cyclones of the Taiwan and Cape Hatteras lows (Agee and Howley, 1977).

Air-sea heat exchange obviously has significant manifestations within the sea as well. For example, Worthington (1977) has postulated that the Gulf stream accelerates after a cold winter as a result of the enhanced differential cross-stream cooling and density gradient. On the other hand Huh[1] has found that the winter heat loss from the Gulf of Mexico takes place episodically during cold air outbreaks and that there is a virtual balance between the cooling of the coastal waters and the heat given up to the atmosphere.

Possible approaches toward the measurement of ocean-air heat fluxes were treated at length at the Jet Propulsion Laboratory/Scripps Institute of Oceanography Workshop on air-sea interaction (NASA, 1980) and the Workshop on Ocean Surface Energetics (Gautier, 1981). One of the key conclusions of the former meeting was that the prospects for the measurement of the fluxes

[1]Private communication from Professor Oscar Huh, Louisiana State University

of heat, moisture, and momentum from space are not promising. This is due to the fact that such fluxes depend upon the profiles of wind, temperature, and moisture in the atmospheric boundary layer, or equivalently, on the bulk transport equations, and there are no clear methods of sensing the required parameters remotely. Only slightly greater optimism was expressed at the second workshop mentioned above.

On the other hand, the fluxes of heat and moisture from sea to air often produce effects which can be observed and which do provide some means of estimating these fluxes. The most obvious products of such fluxes are clouds, the growth of the convective boundary layer, and the warming and moistening of that layer (e.g., Lenchow, 1973). Such effects are especially dramatic in the case of cold air outbreaks over warm waters along the east coasts of Asia and North America (e.g., Ninomiya, 1976; Ninomiya and Akiyama, 1976). There the effects are clearly manifested in the form of cloud streets, as shown in Fig. 1. We see that the upwind (i.e., nearest the shore) edge of the cloud streets is virtually a displaced image of the coastline, the displacement being along the wind direction. It appeared likely that this displacement or distance between shore and the upwind edge of the cloud, here called the "cloud free path" or CFP, is related to the heat and moisture fluxes from the coastal waters such that the greater the fluxes the smaller the CFP. This was essentially our starting hypothesis. In this paper we show that this is indeed the case and develop a method by which one may estimate the fluxes with the aid of the CFP, the sea surface temperature and saturation water vapor mixing ratio, and certain other quantities to be described later.

While the limitations of this study to cold air outbreaks and regions within 200 to 300 km of the coasts would appear rather restrictive, these areas and periods include the major share of the annual global ocean heat losses (Bunker and Worthington, 1976; Agee and Howley, 1977). Kung and Siegel further suggest that the heat transfer from the warm water to the atmosphere in these regions plays a distinct role in the Northern Hemisphere winter circulation.

2. BACKGROUND

Henry and Thompson (1976) inadvertently provided a hint as to how one might use satellite observations to estimate heat fluxes during cold air outbreaks. They used the radiosonde temperature and humidity profiles observed at the coast of the Gulf of Mexico near New Orleans and 24 hours later at Merida, Yucatan, Mexico to deduce the heat fluxes at various points of the trajectory following the cold northerly flow by budget calculation with simple interpolation of temperature and humidity soundings. Well developed cloud streets were evident starting about 100 km south of the Louisiana coast. In their case, the very cold land air of about -4°C over warm Gulf waters of about 20°C produced a total average heat flux of 2400 Wm^{-2} in the first 110 km of travel to a point close to the edge of the first clouds. This is a major flux and again indicates why the problem is important in the previously noted contexts. We shall show later that the fluxes of Henry and Thompson are probably overestimated.

The question at issue, however, is how one can use satellite observations to estimate the heat fluxes without monitoring the temperature and moisture of the air column at both ends of the trajectory as was done by Henry and Thompson. In a preliminary version of this paper, Atlas et al. (1981), hereafter referred to as I, tried several approaches. Their first approach was to use the satellite observed cloud top temperature at initial cloud formation. This temperature could be extrapolated down to near the surface adiabatically, thus providing an estimated sounding which could then be differenced from that measured by radiosonde at the shore to give sensible heating. Similarly, the temperature at cloud formation defines the saturation water vapor mixing ratio which is also well mixed down to near the surface. Comparison to values at the shore would thus provide latent heating. The key assumption in this approach is that the sounding along the trajectory remains unchanged above the flux modified convective boundary layer so that the satellite measured cloud top temperature could be assigned to a known altitude.

While the elements of the concept are sound, its implementation is subject to excessive errors due largely to the small size of the initial clouds relative to the 1 km dimension of the AVHRR (Advanced Very High Resolution Radiometer) IR field of view on the TIROS satellites and the indeterminacy of the temperature correction for unfilled fields of view. These errors are compounded by the large vertical gradient of potential temperature at the inversion so that small errors in determining the temperature of the initial cloud tops, assumed to be at the inversion, translate to large errors in the deduced sounding and thus in net heating. While this method does not work with existing observing systems, it should be kept in mind for possible future application with higher resolution IR imagers and lidar sounders capable of independent cloud height determination.

In I we also utilized the results of Stage (1979) who, with the aid of the boundary layer model of Stage and Businger (1981a, b), computed the potential temperature, vapor mixing ratio, and the height of the convective boundary layer as a function of distance for cold air transports over Lake Ontario. He also calculated the distance from shore to first cloud formation (i.e., the "cloud free path" or CFP), all as a function of varying lake temperatures. It was only necessary then to estimate the sensible and latent heating due to surface fluxes and, with the aid of certain approximations, develop the desired relations to measurable parameters. Because Stage (1979) had only run the Stage-Businger model for a single land air temperature and lapse rate, and for a limited range of lake water temperature, it was not possible to generalize the results in I to a sufficiently wide range of conditions or to determine their limitations. In the present paper we report the generalized results obtained by running the Stage-Businger model over a very broad range of conditions and correct some of the erroneous inferences which were made in I on the basis of more limited data.

In particular, we have developed generalized nomograms of mean column heating due to the surface sensible and latent heat fluxes. The sensible heat nomogram relates the mean sensible heating to the cloud free path (CFP) and the difference between land air and sea surface temperatures, θ_l and θ_0, respectively. The latent heat nomogram relates the mean latent heating to the CFP and the difference between land air and sea surface vapor mixing ratio, q_l and q_0, respectively. The aim, of course, is to estimate the mean sensible and latent heating in the cloud free region from the nomograms using $(\theta_0 - \theta_l)$, $(q_0 - q_l)$ and CFP. The mean surface sensible and latent heat fluxes may then be obtained by multiplying the mean sensible and latent heating by the mean wind speed in the boundary layer.

The sensitivity of the solutions shown in the nomograms to the variations in the initial coastal soundings and large scale subsidence is also investigated. The general behavior of the mean sensible heating, the potential temperature and the height of the boundary layer as a function of downwind distance within the cloud free region and their relations to several important parameters are analyzed in the Appendix.

3. DESCRIPTIONS OF THE BOUNDARY LAYER MODEL

The Stage and Businger (1981a, b) model was developed for the growth and evolution of the marine boundary layer during cold air outbreaks. This is a Lagrangian model. The equivalent potential temperature and the total water mixing ratio are assumed to be well mixed in the boundary layer and are predicted from conservation equations including fluxes from the sea surface and entrainment across the top of the boundary layer. The entrainment rate is determined from the turbulent kinetic energy budget. When clouds form, infrared cooling at cloud top and heating at cloud base are also included. The reality of the model was tested against data gathered during the International Field Year for the Great Lakes (IFYGL). Since our main interest in this paper is the air-mass modification in the cloud free region, only the significant physical processes in the same region are briefly discussed here. The reader is referred to Stage and Businger (1981a, b) for details of the model.

The equations for the cloud free boundary layer are given by

$$d\theta/dt = (\overline{w'\theta'}\,|_0 + W_e \Delta\theta)/Z_B \qquad (1)$$

$$dq/dt = (\overline{w'q'}\,|_0 + W_e \Delta q)/Z_B \qquad (2)$$

$$dZ_B/dt = W_e + W_l \qquad (3)$$

where θ, q, and Z_B are the potential temperature, specific humidity and height of the boundary layer, respectively, d( )/dt the rate of change following a column of air moving at the mean velocity of the mixed layer, $\overline{w'\theta'}\,|_0$ and $\overline{w'q'}\,|_0$ the surface turbulent fluxes, W_e the entrainment rate, W_l the lifting rate of the inversion base due to large scale convergence, and $\Delta\theta$ and Δq correspond to the jumps in θ and q across the base of the inversion. Note that $W_l = -DZ_B$, where D is the large scale divergence and is a prescribed parameter in the model. We shall see that W_l generally appears to have little effect on our results. However, the entrainment rate, W_e, can have considerable influence on the boundary layer through the introduction of warm, dry air from the inversion to the boundary layer. Therefore, a proper determination of W_e is crucial in any mixed layer model. Here W_e is determined from the turbulent kinetic energy budget; i.e., the energy source for the entrainment, which works against buoyancy, is derived from the turbulent kinetic energy of the boundary layer, and this in turn is generated primarily by buoyancy production. In the cloud free region, the surface sensible heat flux plays a very important role in determining W_e.

The surface turbulent fluxes are parameterized according to the bulk transfer formula as

$$\overline{w'\theta'}\,|_0 = C_T\, U\, (\theta_0 - \theta) \qquad (4)$$

$$\overline{w'q'}\,|_0 = C_q\, U\, (q_0 - q) \qquad (5)$$

where θ_0 and q_0 are the sea surface temperature (SST) and the corresponding saturation mixing ratio, respectively, U the mean velocity of the mixed layer, and C_T and C_q the bulk transfer coefficients for heat and moisture, respectively. C_q is taken to be equal to C_T. For the parameterization of the unstable surface layer, the transfer coefficients are independent of wind speed and dependent only on the virtual potential temperature difference between the sea surface and the mixed layer. This is because the transfer coefficients depend only on the ratio of surface roughness to surface layer height, and both are proportional to wind stress. This has the helpful consequence that the downwind profiles of θ, q, and Z_B are independent of wind speed out to the edge of the cloud (Stage, 1979); the wind speed determines only the travel time for the required air-mass transformations. Although some authors have shown transfer coefficients to vary with wind speed, the variation is only slight for unstable conditions such as those under consideration (Kondo, 1975).

4. SENSIBLE AND LATENT HEATING NOMOGRAMS

The *mean* sensible and latent heating between the shore and some downwind distance in the cloud free region are defined as

$$S = \rho c_p \, x^{-1} \int_0^x C_T \, (\theta_0 - \theta) \, dx \tag{6}$$

$$E = \rho L \, x^{-1} \int_0^x C_q \, (q_0 - q) \, dx \tag{7}$$

where x is the distance from the shore along the surface wind direction, ρ the air density, c_p the heat capacity of air at constant pressure, and L the latent heat of condensation. It can be seen from (6) and (7) that S and E are the mean heating of the air column by the warm sea per unit distance of travel as a result of the surface sensible and latent heat fluxes, respectively. It can also be seen from (4) – (7) that the mean surface sensible and latent heat fluxes are equal to SU and EU, respectively. Combining (1), (2), (6) and (7), S and E can be expressed as

$$S = \rho c_p \, x^{-1} \int_0^x (1 + A_\theta)^{-1} \, Z_B \, d\theta \tag{8}$$

$$E = \rho L \, x^{-1} \int_0^x (1 - A_q)^{-1} \, Z_B \, dq \tag{9}$$

where

$$A_\theta = W_e \Delta\theta / \overline{w'\theta'}\,|_0 \tag{10}$$

$$A_q = -W_e \Delta q / \overline{w'q'}|_0 \qquad (11)$$

Here the entrainment coefficients A_θ and A_q are the ratios of the sensible and latent heat fluxes, respectively, at the top of the boundary layer to those at the surface. Without these cross-inversion fluxes, the heat and moisture budgets of the boundary layer would be in gross error. As noted earlier wind speed does not affect the CFP or the downwind profiles of θ, q, and Z_B in the cloud free region. It can be seen from (8) - (11) that S, E, A_θ, A_q, and the nomograms of sensible and latent heating derived with the associated model are independent of wind speed.

In order to construct the nomograms for S and E, several numerical experiments corresponding to the initial soundings shown in Table 1 and θ_0 = 6, 8, ... 26°C for nondivergent flows were performed using the Stage and Businger model. The initial soundings were mainly taken from Stage. The relative humidities (RH) shown correspond to those at the surface. If there is an SST gradient, S and E can be determined from the nomograms using the mean SST of the region of interest for θ_0.

Fig. 2 shows the mean column sensible heating (S) between the shore and 100 km (within the cloud free region) versus the land air-sea surface temperature difference ($\theta_0 - \theta_1$) for nondivergent flow with the initial surface relative humidity of 20% and θ_1 = 3°C. The initial potential temperature lapse rate (Γ_θ) is 3.8°C km^{-1}. It can be seen that S is nearly linearly proportional to ($\theta_0 - \theta_1$). This suggests a new kind of parameterization, i.e., the mean sensible heating is proportional to the horizontal difference rather than the vertical difference of temperature. The slight nonlinearity is mainly due to the weak dependence of C_T on ($\theta_0 - \theta_1$); the change in C_T is about 2% per degree change in ($\theta_0 - \theta_1$). This result, which was evidently overlooked by Stage (1979) and Stage and Businger (1981a, b) because they were not concerned with heat fluxes, has important ramifications in measuring and modeling coastal air-sea interactions since it depends on measurable parameters ($\theta_0 - \theta_1$) rather than on vertical profiles which are often not available. On the other hand, since this finding is itself a result of a model parameterization, it needs to be verified experimentally.

Similarly, Fig. 3 shows the mean column latent heating (E) between shore and 80 km (within the cloud free region) versus the land air-sea surface humidity difference ($q_0 - q_1$) for non-divergent flows. The solid line corresponds to $(\theta_0 - \theta_1) = 11°C$, and the dashed line to $(\theta_0 - \theta_1) = 7°C$, both with $\Gamma_\theta = 3.8°C\ km^{-1}$. It can be seen that E is linearly proportional to $(q_0 - q_1)$ and slightly dependent on $(\theta_0 - \theta_1)$ through the C_q ($= C_T$) dependence. This result also suggests a new parameterization in that the mean latent heating is proportional to the horizontal difference rather than the vertical difference of vapor mixing ratio. Similar comments apply here as were made in connection with the temperature parameterization.

Following the ideas of Figs. 2 and 3 and the analysis shown in the Appendix, the nomograms for estimating the mean sensible (S) and latent heating (E) between shore and the downwind *cloud free* distance (x) under nondivergent conditions are given in Figs. 4 and 5 (solid curves). The solid curves of Fig. 4 show the relation of S to $(\theta_0 - \theta_1)$ and x, while those of Fig. 5 show the relation of E to $(q_0 - q_1)$ and x with weak dependence on $(\theta_0 - \theta_1)$. The application of Figs. 4 and 5 is straight-forward. To obtain the column sensible heating for the cloud free region one enters Fig. 4 with the cloud free path (x = CFP), and the difference between the mean sea surface temperature (θ_0) and the initial shore surface air temperature (θ_1). The SST is readily obtained from the 11 μm channel of the AVHRR on TIROS-N or the same channel on a geosynchronous satellites. In the usually dry cold air outbreaks, little correction is necessary for intervening water vapor. If there is a gradient of SST along the wind direction one may use the average SST between shore and the cloud edge since the heating is essentially linear with $(\theta_0 - \theta_1)$. The value of θ_1 may be obtained from conventional measurements at the shore or from IR measurements of the ground skin temperature empirically corrected to shelter level air temperature. Since the nomograms are produced with a specific value of Γ_θ($= 3.8°C\ km^{-1}$), a correction is also required for other temperature lapse rates at the shore, which should be obtainable from conventional measurements. This correction is discussed in Section 5. Note that Figs. 4 and 5 can also be applied to any region with x < CFP provided that θ_0 is the mean SST for the region concerned.

The use of Fig. 5 for latent heat is analogous to that of Fig. 4. Here q_0 is the saturation mixing ratio at the SST of θ_0. Care must be exerted here in the event of a gradient in SST within x because of the non-linear relation between q_0 and θ_0. The humidity of the initial shore surface air (q_1) can be obtained either from direct measurements or from the dashed curves of Fig. 4, which is to be described shortly. As noted earlier, E depends slightly on $(\theta_0 - \theta_1)$ through the C_q dependence (Fig. 3). Therefore, a correction is required for E to account for the $(\theta_0 - \theta_1)$ dependence. This correction factor may be written as

$$E = E_N(1 + 0.02\,\delta\theta) \tag{12}$$

$$\delta\theta = (\theta_0 - \theta_1)_{obs} - (\theta_0 - \theta_1)_N \tag{13}$$

where the subscripts N and obs denote, respectively, the nomogram and observed values. The heat fluxes for the cloud free region may be obtained simply by multiplying the column heating by the average mixed layer wind speed in the cloud free region. The latter may be estimated by near surface measurements at the shore.

The dashed curves of Figs. 4 and 5 correspond to the CFP for various relative humidities of the initial shore surface air temperature of 3°C. Although large scale subsidence and the initial lapse rates of temperature and humidity at the shore also affect the CFP, the dashed curves of Fig. 4 suggest that, to a first approximation, CFP and $(\theta_0 - \theta_1)$ can be used to determine q_1 for a known θ_1. As mentioned above q_1 is required in using Fig. 5 to obtain the latent heating if one does not have a direct humidity measurement. Indeed, because of the notable errors in radiosonde measurements of humidity, this approach may turn out to be more accurate once the theoretical results are validated experimentally.

Note also that the cloud free path should be measured by a geosynchronous satellite either in the visible or IR because it varies diurnally with the land air temperature (see Section 6). Both Figs. 4 and 5 are valid only for x within the cloud free region. While Fig. 4 shows that sensible heating is not especially sensitive to x (the variation in S is about 10% per 100 km uncertainty in x for a constant $(\theta_0 - \theta_1)$ curve), one needs the CFP to determine the average SST (θ_0) in the cloud free region when there is an SST gradient.

An examination of Figs. 4 and 5 shows the following key features within the cloud free region:

(1) For constant x, S increases essentially linearly with increasing $(\theta_0 - \theta_1)$ and E with $(q_0 - q_1)$.

(2) For constant $(\theta_0 - \theta_1)$, S decreases by 30 to 35% for x ranging from 0 to 300 km. For constant $(\theta_0 - \theta_1)$ and $(q_0 - q_1)$, E also decreases with increasing x. As the dry cold air travels over a warmer sea with a constant SST, the air becomes warmer and wetter and the local air-sea temperature and humidity differences are gradually reduced; hence S and E decrease gradually.

(3) For the same initial temperature and humidity soundings, an increase in SST causes an increase in S and E but a decrease in CFP; i.e., fluxes increase and clouds form sooner.

(4) For constant θ_1 and θ_0, a decrease in the relative humidity of the initial land air causes an increase in CFP and E of the cloud free region but a decrease in S of this region.

Although the nomograms are generated with $\theta_1 = 3°C$, its generality can be seen from the analysis shown in the Appendix and the numerical solutions shown in Fig. 6. The solid curves of Fig. 6 show the downwind variation of the mean sensible heating, the local vertical air-sea temperature difference, and boundary layer height for the case of 20% RH with $\theta_1 = 3°C$, $(\theta_0 - \theta_1)$

$= 11°C$ and $\Gamma_\theta = 3.8°C\ km^{-1}$. For this case the cloud free path is 280 km. The symbols along the curves show values of S, $(\theta_0 - \theta)$, and Z_B at the cloud edge for other initial temperature and humidity conditions of the land air but with the same values of $(\theta_0 - \theta_1)$ and Γ_θ. We note that the initial temperature soundings for the 80% and 60% RH cases and the initial humidity soundings for the cases of $\theta_1 = -10°$ and $\theta_1 = -7°C$ are the same as those for the case of 20% RH and $\theta_1 = 3°C$.

It can be seen that the profiles of $(\theta_0 - \theta)$, S and Z_B in the cloud free region are virtually independent of the initial temperature and humidity soundings provided that $(\theta_0 - \theta_1)$ and Γ_θ are fixed. (The effects of Γ_θ are discussed in Section 5). However, the cloud free path indicated by the position of the various symbols is highly sensitive to the initial soundings, i.e., clouds form sooner at higher RH. This confirms our previous findings, namely that the mean sensible heating for the cloud free region is uniquely determined by $(\theta_0 - \theta_1)$, Γ_θ, and CFP. We shall see that this is also consistent with the analysis in the Appendix. The fact that the boundary layer growth in the cloud free region is almost totally controlled by the surface sensible heat flux, and thus also by $(\theta_0 - \theta_1)$ and Γ_θ, is also significant since the boundary layer height is a parameter which should also be measurable from space. Indeed, other things being equal, the growth rate of the boundary layer and sensible heating may be used as proxies for one another. Eq. (A15) in the Appendix shows that the sensible heating is directly proportional to the average value of $d(Z_B^2)/dx$ in the cloud free region. We shall discuss this further below.

Our analyses also indicated that the mean latent heating for the cloud free region may be determined nearly uniquely from a knowledge of $(q_0 - q_1)$, $(\theta_0 - \theta_1)$, Γ_θ and CFP. For a fixed $(\theta_0 - \theta_1)$, $(q_0 - q_1)$ and Γ_θ, the mean latent heating in the cloud free region was found to be slightly dependent on the initial humidity lapse rate, Γ_q. However, the effect is very small, as can be seen from Table 2, which shows the percentage errors in S and E at 100 km from the coast due to errors in various factors. The percentage errors in S and E due to an error of 1°C in $(\theta_0 - \theta_1)$ and of 1 g kg^{-1} in $(q_0 - q_1)$ are smaller for larger $(\theta_0 - \theta_1)$ and $(q_0 - q_1)$, respectively. They amount to about 11% in S for $(\theta_0 - \theta_1) = 9 - 11°C$ and 15% in E for $(q_0 - q_1) = 6 - 8$ g kg^{-1}. A 10 km uncertainty in CFP causes about a 1% and a 0.5% error in S and E, respectively. A 10^{-5} s^{-1} uncertainty in the divergence causes about a 0.2% and a 0.03% error in S and E, respectively. This suggests that the nomograms (Figs. 4 and 5) generated from the nondivergent flow may generally be used to estimate S and E for divergent flows.

5. EFFECTS OF INITIAL POTENTIAL TEMPERATURE LAPSE RATE

For a constant θ_1, an initial land air column associated with a large Γ_θ is warmer than that with a small Γ_θ. After modification from below by warmer water the former tends to maintain a warmer temperature in the boundary layer and thus produces a smaller driving force for the sensible heat flux. In spite of the smaller sensible heating with larger Γ_θ the boundary layer always remains warmer because of its shallower depth as compared to that with small Γ_θ. Therefore, for a fixed $(\theta_0 - \theta_1)$, S decreases with increasing Γ_θ. Similarly, for a fixed $(\theta_0 - \theta_1)$ and $(q_0 - q_1)$, E also decreases with increasing Γ_θ.

For Γ_θ greater than 3.8°C km^{-1}, the sensible heating nomogram (Fig. 4) overestimates the sensible heating and thus requires a negative correction factor, and conversely. According to our analysis, the Z_B-normalized correction factor for the mean sensible heating may be approximated as (see Appendix)

$$(\Delta S/S)/Z_B \simeq -0.25\ [(1 + A_\theta)/(1 + 2A_\theta)]\ [(\Gamma_\theta - 3.8)/(\theta_0 - \theta_1)] \qquad (14)$$

Here Z_B is the boundary layer height at the downwind edge of the region in which S is computed, and A_θ the entrainment coefficient of potential temperature defined in (10) as the ratio of sensible heat flux at the top of the boundary layer to that at the surface. The value of A_θ computed from Stage and Businger's model is generally about 0.3 in the cloud free region for $(\theta_0 - \theta_1) >$ 7°C. Note that the entrainment coefficient of *virtual* potential temperature is equal to 0.2 in the same model. These two entrainment coefficients are in reasonable agreement with those obtained in other studies (e.g., Tennekes, 1973; Willis and Deardorff, 1974; Randall, 1980). Figs. 7 and 8 show the Z_B-normalized correction factors for the mean sensible heating, $(\Delta S/S)/Z_B$, and the mean latent heating, $(\Delta E/E)/Z_B$ versus Γ_0 for various $(\theta_0 - \theta_1)$ as derived from the results of numerical experiments. It can be seen that Fig. 7 is consistent with (14) and that the Z_B-normalized errors increase with increasing deviation of Γ_0 from 3.8°C km^{-1}, and decrease with increasing $(\theta_0 - \theta_1)$. The correction factors $(\Delta S/S)$ and $(\Delta E/E)$ for the cloud free region may be obtained by multiplying the ordinates by Z_B (km) at the cloud edge. The boundary layer height may be measured by a variety of ground based remote sensors such as lidar or sensitive microwave radars. In the future, it should be measurable by a spaceborne lidar scattering off the sea salt aerosols at the top of the convective boundary layer.

According to our analysis, the boundary layer slope within the cloud free region under nondivergent conditions may be written as (see Appendix)

$$dZ_B/dx = [(1 + 2A_0)(\theta_0 - \theta_1)/(\Gamma_0 Z_B) - (1 + A_0)]\ C_T \tag{15}$$

For large $(\theta_0 - \theta_1)$ and small Γ_0 and Z_B, (15) may be approximated as

$$dZ_B^2/dx \simeq 2(1 + A_0)C_T\ (\theta_0 - \theta_1)\ /\Gamma_0 \tag{16}$$

Eq. (16) suggests that Γ_0 may be estimated from a knowledge of $d(Z_B^2)/dx$ and $(\theta_0 - \theta_1)$. Fig. 9 shows the slope of Z_B^2 versus Γ_0 for various $(\theta_0 - \theta_1)$ under nondivergent conditions as derived from the results of the numerical experiments. Here $d(Z_B^2)/dx$ is determined from the first 50 km within the cloud free region (or from the cloud free region if the CFP is smaller than 50 km). It can be seen that $d(Z_B^2)/dx$ increases with increasing $(\theta_0 - \theta_1)$ and decreases with increasing Γ_0, which is consistent with (16). For nondivergent flow, the potential temperature lapse rate for the unmodified air (i.e., above the convective boundary layer) at time t, $\gamma_0(t)$, is the same as that of the initial sounding, Γ_0. For divergent flow, $\gamma_0(t)$ is gradually increased by the divergence and may be given as (Carson, 1973)

$$\gamma_0 \text{ (t)} = \Gamma_0 \exp \text{(Dt)} \qquad (17)$$

where D is the divergence. Therefore, divergence tends to decrease Z_B by increasing the potential temperature lapse rate. However, the effects of divergence on $d(Z_B{}^2)/dx$ are expected to be very small for the first 50 km or the first hour of travel.

6. OBSERVATIONS

Fig. 10 shows a TIROS-N AVHRR IR image for a cold air outbreak on 17 February 1979 at 1941 GMT. The cloud streets are aligned essentially along the wind direction, from the north and northwest, as seen from the winds at the three buoys as sown in Fig. 11. Initial cloud formation typically occurs about 100 km off the nearest upwind shore so that the boundary of the clouds is virtually an image of the coastline. South of Long Island, New York, the image shows surface water temperatures increasing from about -1.5°C at the shore to 2°C about 50 km south. Approximately 500 km south of Long Island (36°N latitude), the clouds become solid and are extremely uniform in the east-west direction over a distance of about 1100 km. Note that the coldest cloud top temperatures of –21°C (dark green) occur at latitude 38°N where the clouds remain in the form of streets. Although it is almost certain that the cloud tops continue to grow southward of the coldest point, the top temperatures grow progressively warmer. This is due to the growth of the clouds into the inversion layer so that higher clouds are associated with warmer temperatures.

Fig. 11 shows the surface weather map at 1500 GMT (1000 EST), about 5 hours earlier than the time of TIROS-N AVHRR picture (Fig. 10). A high pressure system centered in the Great Lakes area dominates the entire east coast of North America. Cloud street orientation is generally observed to be along the mean wind in the planetary boundary layer and about 15° to the left of the surface geostrophic wind (Lemone, 1973). This is also consistent with the case of

17 February 1979. Fig. 12 shows the weekly mean SST for the period of 14-21 February 1979. The temperatures are seen to be slightly warmer than the AVHRR IR brightness temperatures for the cloud free coastal region. Note that the air flows across the SST isotherms for the region from Maine to Long Island, where the cloud streets are best organized. Further south, the air flow is nearly parallel to the SST isotherms. Also note the moderate snowfall (Fig. 11) reported at Cape Hatteras, the snow quite obviously having originated in the low level clouds formed over the relatively warm sea.

In order to examine the present method the case of 17 February 1979 was fully analyzed and the sensible heating derived from the nomogram (Fig. 4) was then compared to that computed from the bulk transfer formula. A buoy located at about 75 km downwind from the Long Island shore (40.1°N, 73°W) and several coastal stations provided hourly air (T_a) and sea surface temperatures (T_s) and wind speed (U) for the computation of sensible heat flux (SH) with the bulk transport formula, which is

$$SH = \rho c_p C_H (T_s - T_a) U \tag{18}$$

Here C_H is the bulk transfer coefficient for the sensible heat flux, and is taken to be 1.5×10^{-3} (Kondo, 1975) for the diurnal ranges of temperature and wind in this case. Note that this value of C_H is consistent with that of C_T generated in Stage and Businger's model, which is about $1.5 \sim 1.6 \times 10^{-3}$ for this kind of situation ($(\theta_0 - \theta_1) \sim 15 - 19$°C). The sensible heat fluxes at the shore and at the buoy were computed from (18). The mean sensible heating was then computed by dividing the mean sensible heat flux by the mean wind speed between the shore and the buoy.

The cloud free path, averaged over about 120 km wide coastal region south of Long Island, was measured manually from the hourly GOES-2 IR cloud pictures. Because the mean sensible heating for the cloud free region discussed in Section 4 is the average along the trajectory in a Langrangian sense, and the manually measured CFP is fairly subjective, a three-point running mean was applied to all the data (CFP, U, T_s and T_a). In order to estimate the mean sensible heating for the cloud free region from the nomogram, we need both $(\theta_0 - \theta_1)$ and the CFP. Since it takes time for the initial land air to form the first cloud downstream, we used values of θ_1 observed at the shore at times earlier than the cloud observations differing by the travel time from shore to cloud edge corresponding to the mean wind speed between the shore and the buoy. The mean SST for the cloud free region, θ_0, was determined from the CFP and the coastal SST field, which was estimated from the SST at the coastal station and the buoy. The coastal SST field was found to have a gradient of about 0.07°C km^{-1} and was rather steady.

Fig. 13 shows the diurnal variations of cloud free path (circles) and the associated mean sensible heating for the 17 February 1979 cold air outbreak south of the Long Island, New York coast. The solid curve is the mean sensible heating between the shore and the buoy (75 km) computed from the bulk transfer formula, while the squares represent the mean sensible heating between the shore and the cloud edge (60 to 120 km) estimated from the sensible heating nomogram (i.e., Fig. 4). Note that the errors in the nomogram estimates due to divergence and the initial potential temperature lapse rate (Γ_θ) are probably fairly small because of the small divergence (1.5×10^{-5} sec^{-1}) and large values of $(\theta_0 - \theta_1)$ (about 15 – 19°C for most of the data) and the small deviation of Γ_θ from 3.8° km^{-1} (Γ_θ is about 1.3 – 1.8°C km^{-1}).

We see that the results obtained from the present method are generally in very good agreement with those from the bulk transfer formula. Since there is no diurnal variation in the coastal SST field as evidenced both at the shore station (Fire Island) and the buoy, the variation in the mean sensible heating between the shore and the buoy is due mainly to the variation in the initial shore surface air temperature (θ_1). The initial shore surface air temperature varies from a minimum of −18°C around 0700 EST to a maximum of −10°C near 1500 EST. Note that the maximum of S (between shore and the buoy) generally corresponds to the coldest land air temperature and vice versa. On the other hand, there is a slight diurnal variation in the mean SST over the cloud free region (θ_0 varies from 1.2 to 3.8°C) because of the gradient of SST (about 0.07°C km^{-1}) and the variation in CFP. This is due only to the fact that the varying cloud edge is the outer limit over which θ_0 is averaged. In short, the variation in S in the cloud free region is due to the variation in the initial shore surface air temperature, θ_1, and the change in the effective SST, θ_0. For a CFP smaller than 75 km, S of the cloud free region (squares) is generally smaller than that of the region between the shore and the buoy (solid curve), because the effective θ_0 is smaller in the former than in the latter. For CFP larger than 75 km, the reverse is true. This accounts for most of the difference between the present and the conventional methods of estimating heat flux.

The daily averages of S and SH computed from the bulk transfer formula are about 25 J m^{-3} and 249 W m^{-2}, respectively, with the observed daily mean wind speed of about 10 ms^{-1}. These values agree almost identically with the average values obtained from the nomogram. Although Fig. 13 indicates that S is overestimated after 1200 GMT for the reason noted above, these were balanced by the underestimates prior to that time, thus giving excellent agreement for the daily averages.

The present method was also applied to the case of the cold air outbreak analyzed by Henry and Thompson (1976). The values of θ_0, θ_1, q_0, q_1, CFP, and U were chosen to be 20°C, −4°C, 14.5 g kg^{-1}, 1 g kg^{-1}, 100 km and 10 ms^{-1}, respectively. The corresponding sensible and latent heat fluxes estimated from the nomograms were 400 and 600 W m^{-2}, respectively, for the cloud free region with a travel time of about 3 hours. These values are much smaller than those obtained by Henry and Thompson. The sensible and latent heat fluxes are about 27% and 72%, respectively, of their corresponding values. Since the temperature and humidity soundings near the cloud edge used by Henry and Thompson were estimated, not observed, it is likely that the estimated soundings were too warm and too wet, thus producing excessive apparent sensible and latent heat fluxes. Also, the heating and drying effects of entrainment through the top of the boundary layer, which are important in the heat and moisture budgets, are not included in the Henry and Thompson budget calculation. This is surely another major cause of the discrepancy.

7. CONCLUSIONS AND DISCUSSION

In the present paper we have shown how the sensible and latent heating of the atmosphere due to surface fluxes is related to the downwind distance offshore at which clouds first form during cold air outbreaks over the warmer coastal waters. This distance, the so-called cloud free path or CFP, and the mean sea surface temperature, both of which are measurable from space, along with the temperature and moisture content of the initial shore surface air, both measurable by conventional means, are all that are required to utilize the nomograms (Figs. 4 and 5) developed here. Other things being equal, the greater the land air-sea surface temperature contrast, the greater the heat and moisture fluxes and the closer to shore the clouds will form.

The results are not sensitive to flow divergence or to initial lapse rate of humidity at the shore, but are dependent upon the initial lapse rate of potential temperature, Γ_θ. If this is not known from conventional soundings at the shore, it may be deduced from the downwind slope of the square of the boundary layer height (Z_B^2) which is proportional to the land air-sea surface temperature difference and inversely proportional to Γ_θ. The mean slope of (Z_B^2) is also directly proportional to sensible heating so that it may be used as a proxy for the latter. The slope of the boundary layer height may be measured by a variety of ground based remote sensors such as lidar, acoustic radar, or sensitive microwave radars. In the future, we expect that it will also be measurable by spaceborne lidar scattering off the sea salt aerosols at the top of the convective boundary layer. Another important future step is to extend the present approach further from the coast beyond the cloud edge because it is clear that significant heating continues to occur after clouds have formed (Henry and Thompson, 1976).

Within the cloud free region, the profiles of potential temperature, water vapor mixing ratio and the height of the boundary layer along the wind direction were found to be independent of wind speed. This also makes the downwind profiles of the mean sensible and latent heating independent of wind speed. The generality of these results needs to be investigated further through the comparison with other models (e.g., Brost, 1976, Randall, 1980, Moeng and Arakawa, 1980) and empirical studies. The various models may have different values of the entrainment coefficients. Theoretical analyses (see Appendix) suggest that the growth and heating of the boundary layer within the cloud free region are not sensitive to the variation in the entrainment coefficient (A_θ) so long as it is within a reasonable range. If the parameterization of the turbulent transfer coefficients through the air-sea interface is similar to that in Stage and Businger's model, it is expected that the model dependency of the nomograms will be very small. Nevertheless, we recommend validation experiments and fine tuning of our results before they are applied more broadly.

The method was tested in two cases. The first one showed good agreement in sensible heating as compared with that computed from buoy measurements and the bulk transfer formula. However, a major discrepancy was found in our comparison to the case reported by Henry and Thompson (1976) due to factors discussed earlier.

There are some interesting by-products of this work which are worth noting. First of all, the model results indicate that the sensible heat flux is almost linear with the land air-sea surface temperature difference, and that the latent heat flux is linear with the land air-sea surface vapor mixing ratio difference, the latter with a small correction for the temperature difference. This suggests the possibility of a new kind of flux parameterization for the convectively unstable case which depends upon the horizontal differences across the coast instead of upon the vertical differences as in the classical bulk transfer equations.

Another interesting aspect of the present work is that it appears that the method can be used in reverse to check the validity of some of the basic assumptions and features of boundary layer models. For example, it would be useful to determine whether or not the CFP and the other parameters (θ, q, Z_B, S and E) on which it depends are indeed independent of the wind speed as the Stage and Businger (1981a, b) model suggests. In addition, observations such as these should permit an indirect determination of the overall validity of models such as that used here. While it may not be possible to separate the effects of various processes or parameters in the boundary layer model, the position of the first cloud formation should provide fairly sensitive tests of its overall performance.

Finally, it is evident that the physical processes and results discussed here are related to the lake-effect snowstorms observed on the leeward side of lakes during cold outbreaks (Lavoie, 1972; Passarelli and Braham, 1981). It seems likely that our method should be adaptable to the nowcasting of such snowfalls since the snowfall rate is related to the net moisture flux, or the difference between that coming from the lake (ocean) surface and that transported across the inversion. It is of interest that both these important moisture supply and loss terms are automatically incorporated in determining the cloud free path.

8. ACKNOWLEDGEMENTS

We are most grateful to Dr. Steven A. Stage of Florida State University and Professor Joost Businger of the University of Washington for having given us their model and computer code; to Dr. Paul Hwang of NASA/Goddard Laboratory for Atmospheric Sciences (GLAS) for wide ranging assistance, and to Mr. William Byerly of Systems and Applied Sciences Corporation for his enthusiastic effort on programming and data analysis. Our gratitude is also extended to Drs. David Randall and Ming-Dah Chou of GLAS and Dr. Chin-Hoh Moeng of Sigma Data Corporation and GLAS for helpful discussions and criticism. We also appreciate the general assistance of Mr. Earl Kreins and the fine typing and editorial work of Mrs. Sharon Anderson, both of GLAS. The second author wishes especially to acknowledge the assistance of Mr. William R. Bandeen, Associate Chief of GLAS, for relieving him of his managerial responsibilities so that he could conduct this research.

APPENDIX

Analytical Formulation for the Cloud Free Region

The heat budget equation for the cloud free boundary layer may be written as

$$d\theta/dt = (\overline{w'\theta'}\,|_0 + W_e\Delta\theta)/Z_B \tag{A1}$$

where θ and Z_B are the potential temperature and height of the boundary layer, respectively, t time, $\overline{w'\theta'}\,|_0$ the surface turbulent flux of potential temperature, W_e the entrainment rate, and $\Delta\theta$ the jump of θ across the inversion base. For nondivergent conditions ($dZ_B/dt = W_e$), (A1) may be rewritten as

$$d\theta/dZ_B = [(1 + A_\theta)/A_\theta]\,(\Delta\theta/Z_B) \tag{A2}$$

where the entrainment coefficient is given by

$$A_\theta = W_e\,\Delta\theta/\overline{w'\theta'}\,|_0 \tag{A3}$$

The jump in potential temperature at the inversion base may be given as

$$\Delta\theta = \theta_1 + \Gamma_\theta\,Z_B - \theta \tag{A4}$$

where θ_1 is the initial surface potential temperature at the shore and Γ_θ the initial potential temperature lapse rate. Using (A4), (A2) may be rewritten as

$$d\theta/dZ_B = [(1 + A_\theta)/A_\theta]\,[\Gamma_\theta - (\theta - \theta_1)/Z_B] \tag{A5}$$

which may be integrated to give

$$\theta = \theta(0)M + \theta_1(1 - M) + [(1 + A_\theta)/(1 + 2A_\theta)]\,\Gamma_\theta\,[Z_B - Z_B(0)\,M] \tag{A6}$$

$$M = [Z_B/Z_B(0)]^{-[(1 + A_\theta)/A_\theta]}$$

where $\theta(0)$ and $Z_B(0)$ are the initial potential temperature and height of the mixed layer, respectively. Note that the initial temperature sounding is generally stable and $Z_B(0)$ is very small. For the convectively unstable boundary layer, A_θ is generally about 0.3 in the cloud free region and Z_B is generally much larger than $Z_B(0)$. Therefore (A6) becomes

$$\theta \simeq \theta_1 + [(1 + A_\theta)/(1 + 2A_\theta)] \; \Gamma_\theta Z_B \tag{A7}$$

Eq. (A7) is a linear relationship between the potential temperature and height of the convective boundary layer in the cloud free region.

Eq. (A1) may also be written as

$$d\theta/dt = (1 + A_\theta) \overline{w'\theta'}\,|_0 \;/Z_B \tag{A8}$$

where

$$\overline{w'\theta'}\,|_0 = C_T \, U(\theta_0 - \theta) \tag{A9}$$

C_T is the bulk transfer coefficient, U is the mean wind speed in the boundary layer, and θ_0 is the sea surface temperature.

Combining (A8) and (A9), results in

$$d\theta/dx = C_T (1 + A_\theta) (\theta_0 - \theta)/Z_B \tag{A10}$$

Where x is the distance from the shore along the wind direction.

Combining (A7) and (A10), results in

$$dZ_B/dx = [(1 + 2A_\theta)(\theta_0 - \theta_1)/(\Gamma_\theta Z_B) - (1 + A_\theta)] \; C_T \tag{A11}$$

For large $(\theta_0 - \theta_1)$ or small Γ_θ and Z_B, (A11) may be approximated as

$$dZ_B/dx = C_T(1 + 2A_\theta) (\theta_0 - \theta_1)/(\Gamma_\theta Z_B) \tag{A12}$$

which may be integrated to give

$$Z_B{}^2 = Z_B{}^2(0) + 2\,\overline{C}_T\,(1 + 2A_\theta)\,(\theta_0 - \theta_1)\,x/\Gamma_\theta \tag{A13}$$

where

$$\overline{C}_T = x^{-1} \int_0^x C_T\,dx$$

The mean sensible heating between the shore and some downwind distance in the cloud free region is defined as

$$S = \rho c_p\, x^{-1} \int_0^x C_T\,(\theta_0 - \theta)dx \tag{A14}$$

Using (A7) and (A10), (A14) may be expressed as

$$S = \rho c_p\, x^{-1} \int_0^x [0.5\Gamma_\theta/(1 + 2A_\theta)]\;[dz_B{}^2/dx]\;dx \tag{A15}$$

Eq. (A15) indicates that the sensible heating in the cloud free region is directly proportional to the average value of $d(Z_B{}^2)/dx$ in the same region. This supports the earlier statement that the sensible heating and the growth rate of the boundary layer are proxies for one another. Using (A11), (A15) may also be expressed as

$$S = \rho c_p\,\overline{C}_T\,(\theta_0 - \theta_1) - 0.5\,\rho c_p\,\overline{C}_T\,\Gamma_\theta\,Z_B\,(1 + A_\theta)/\,(1 + 2A_\theta) \tag{A16}$$

From (A11) and (A16) we see that S can be uniquely determined by $(\theta_0 - \theta_1)$, Γ_θ and x. Note also that the second term of the R.H.S. of (A16) is generally much smaller than the first term. Using (A13) and (A16), the fractional error in S due to the change in Γ_θ may be approximated as

$$(\partial S/\partial\Gamma_\theta)/S \simeq -0.25\,[(1 + A_\theta)/(1 + 2A_\theta)]\;[Z_B/(\theta_0 - \theta_1)] \tag{A17}$$

As mentioned earlier, A_θ computed from Stage and Businger's model is generally about 0.3 in the cloud free region for $(\theta_0 - \theta_1) > 7°C$. It can be seen from (A7), (A13) and (A16) that an increase of A_θ from 0.2 to 0.4 causes a 13% increase in Z_B, a 3% increase in $(\theta - \theta_1)$ and a 3% decrease in $[S - \rho c_p \overline{C}_T (\theta_0 - \theta_1)]$. This suggests that our results are insensitive to A_θ and that the model dependency of the nomograms is almost completely controlled by the parameterizations of the turbulent transfer through the air-sea interface, particularly upon the transfer coefficients.

REFERENCES

Atlas, D., S. H. Chou, and P. Hwang, 1981: Estimating heat transport over coastal waters from cloud street signatures. Proceedings of a Workshop on Applications of Existing Satellite Data to the Study of the Ocean Surface Energetics, 19-21 November 1980. Report, NASW-57380 February 1981, University of Wisconsin Press, 49-60.

Agee, E. M., and R. P. Howley, 1977: Latent and sensible heat flux calculations at the air-sea interface during AMTEX 74. *J. Appl. Meteor.*, *16*, 443-447.

Bjerknes, J., 1966: A possible response of the atmospheric Hadley circulation to equatorial anomalies of ocean temperature. *Tellus*, *28*, 820-828.

__________, 1969: Atmospheric teleconnections from the equatorial Pacific. *Mon. Wea. Rev.*, *97*, 163-172.

Brost, R. A., 1976: Air mass modification in the atmosphere's boundary layer: A study using a two dimensional numerical model with a higher order turbulence closure. Ph.D. thesis in meteorology, University of Wisconsin, Madison.

Bunker, A., and L. V. Worthington, 1976: Energy exchange charts of the North Atlantic Ocean. *Bull. Amer. Meteor. Soc.*, *57*, 450-467.

Carson, D. J., 1973: The development of a dry inversion-capped convectively unstable boundary layer. *Quart. J. R. Meteor. Soc.*, *99*, 450-467.

Gautier, C., 1981: Proceedings of a Workshop on Applications of Existing Satellite Data to the Study of the Ocean Surface Energetics, 19-21 November 1980. Report, NASW-57380, February 1981, University of Wisconsin Press.

Henry, W. K., and A. H. Thompson, 1976: An example of polar air modification over the Gulf of Mexico. *Mon. Wea. Rev.*, *104*, 1324-1327.

Kondo, J., 1975: Air-sea bulk transfer coefficients in diabatic conditions. *Boundary Layer Meteor.*, 9, 91-112.

Kung, E. C., and A. J. Siegel, 1979: A study of heat and moisture budgets in the intense winter monsoon over the warm ocean current. *J. Atmos. Sci.*, *36*, 1880-1894.

Lavoie, R. L., 1972: A mesoscale numerical model of lake-effect storms. *J. Atmos. Sci.*, *29*, 1025-1040.

LeMone, M. A., 1973: The structure and dynamics of horizontal roll votices in the planetary boundary layer. *J. Atmos. Sci.*, *30*, 1077-1091.

Lenchow, D. H., 1973: Two examples of planetary boundary layer modification over the Great Lakes, *J. Atmos. Sci.*, *30*, 568-581.

Moeng, C. H., and A. Arakawa, 1980: A numerical study of a marine subtropical stratus cloud layer and its stability. *J. Atmos. Sci.*, *37*, 2661-2676.

Namias, J., 1969: Seasonal interactions between the North Pacific Ocean and atmosphere during the 1960's. *Mon. Wea. Rev.*, *97*, 173-192.

__________, J., 1978: Multiple causes of the North America abnormal winter 1976-77. *Mon. Wea. Rev.*, *106*, 279-295.

NASA, 1980: Guidelines for the air-sea interaction special study: An element of the NASA Climate Research Program. NASA/Jet Propulsion Laboratory, JPL Publication 80-8, Feb. 15, 1980.

Ninomiya, K., 1976: Large-scale heat and moisture budget during the Air-Mass Transformation Experiment. *J. Meteor. Soc. Japan, 54*, 1-14.

__________ and T. Akiyama, 1976: Structure and heat energy budget of mixed layer capped by inversion during the period of polar outbreak over Kuroshio region. *J. Meteor. Soc. Japan, 54*, 117-131.

Passarelli, Jr., R. E., and R. R. Braham, Jr., 1981: The role of the winter land breeze in the formation of Great Lake snow storm. *Bull. Amer. Meteor. Soc.*, *62*, 482-491.

Randall, D. A., 1980: Entrainment into a stratocumulus layer with distributed radiative cooling. *J. Atmos. Sci.*, *37*, 148-159.

Sheu, P. J., and E. M. Agee, 1977: Kinematic analysis and air-sea heat flux associated with mesoscale cellular convection during AMTEX 75. *J. Atmos. Sci.*, *34*, 793-801.

Stage, S. A., 1979: A model for modification of the cloud-topped marine boundary layer during cold air outbreak. Dept of Atmospheric Sciences, University of Washington, 280 pp.

__________, and J. A. Businger, 1981a: A model for entrainment into a cloud-topped marine boundary layer—Part I: Model description and application to a cold air outbreak episode. Manuscript submitted to the *J. Atmos. Sci.*

________ *and* _______ , 1981b: A model for entrainment into a cloud-topped marine boundary layer—Part II: Discussion of model behavior and comparison with other models. Manuscript submitted to the *J. Atmos. Sci.*

Tennekes, H., 1973: A model for the dynamics of the inversion above a convective boundary layer. *J. Atmos. Sci.*, *30*, 558-567.

Warsh, K. L., 1973: Relation of air-sea interface energy fluxes to convective activity in the tropical Atlantic Ocean. *J. Geophys. Res.*, *78*, 504-510.

Willis, G. E., and J. W. Deardorff, 1974: A laboratory model of the unstable planetary boundary layer. *J. Atmos. Sci.*, *31*, 1297-1307.

Worthington, L. V., 1977: Intensification of the Gulf Stream after the winter of 1976-77. *Nature*, *270*, 415-417.

TABLE 1. Initial soundings

$$\theta = \theta_1 + \Gamma_\theta Z$$

$$q = q_1 + \Gamma_q Z$$

Relative Humidity (%)	θ_1 (°C)	Γ_θ (°C km^{-1})	q_1 (g kg^{-1})	Γ_q (g kg^{-1} km^{-1})
80	3	3.8	3.6	−0.68
75	3	3.8	3.4	−0.75
60	3	3.8	2.7	−0.51
40	3	3.8	1.8	−0.34
20	3	3.8	0.9	−0.17
50	− 10	3.8	0.9	−0.17
40	− 7	3.8	0.9	−0.17

TABLE 2. Errors in sensible and latent heatings at 100 km from the shore.

FACTORS	ERRORS	$\Delta S/S$ (%)	$\Delta E/E$ (%)	REMARKS
$(\theta_0 - \theta_1)$	1°C	25		$(\theta_0 - \theta_1) = 3 - 5°C$
$(\theta_0 - \theta_1)$	1°C	11		$(\theta_0 - \theta_1) = 9 - 11°C$
$(\theta_0 - \theta_1)$	1°C	8		$(\theta_0 - \theta_1) = 15 - 17°C$
$(\theta_0 - \theta_1)$	1°C		2	$(\theta_0 - \theta_1) = 3 - 23°C$, No Errors in $(q_0 - q_1)$
$(q_0 - q_1)$	1 g kg^{-1}	0	15	$(\theta_0 - \theta_1) = 11°C$, $(q_0 - q_1) = 6 - 8$ g kg^{-1}
Γ_θ	1 g kg^{-1}	0	5	$(\theta_0 - \theta_1) = 11°C$, $(q_0 - q_1) = 7.8$ g kg^{-1}, $\Gamma_q = 0.17 - 0.51$ g kg^{-1} km^{-1}
CFP	10 km	1	0.5	$(\theta_0 - \theta_1) = 3 - 21°C$
D	10^{-5} s^{-1}	0.2	0.03	$(\theta_0 - \theta_1) = 11°C$, $(q_0 - q_1) = 7.8$ g kg^{-1} $\Gamma_q = 0.34$ g kg^{-1} km^{-1}

FIGURE CAPTIONS

Figure 1. Cold air outbreak on 3 January 1979 as seen by GOES-2 visible channel. Note that shoreward edge of clouds is nearly an image of the coastline.

Figure 2. Mean column sensible heating (S) between shore and 100 km versus land air-sea surface temperature difference $(\theta_0 - \theta_1)$ for an initial surface RH of 20% with θ_1 = 3°C and initial potential temperature lapse rate (Γ_θ) of 3.8°C km^{-1}.

Figure 3. Mean column latent heating (E) between shore and 80 km versus land air-sea surface humidity difference $(q_0 - q_1)$. Solid line corresponds to $(\theta_0 - \theta_1)$ = 11°C, and dashed line to $(\theta_0 - \theta_1)$ = 7°C. All for the initial potential temperature lapse rate (Γ_θ) of 3.8°C km^{-1}. Symbols in legend correspond to various initial soundings.

Figure 4. Mean column sensible heating (S) between shore and downwind cloud free distance (x) versus x for various land air-sea surface temperature differences $(\theta_0 - \theta_1)$ under nondivergent conditions and initial potential temperature lapse rate of 3.8°C km^{-1} (solid lines). Dashed lines correspond to the cloud free paths for various surface relative humidities (RH) and initial shore surface air temperature (θ_1) of 3°C. Each cross indicates a numerical experiment.

Figure 5. Sames as Fig. 4, except for the dependence of mean column latent heating (E) on land air-sea surface humidity difference $(q_0 - q_1)$ and land air-sea surface temperature difference $(\theta_0 - \theta_1)$. Equation at bottom shows corrections in E due to values of $(\theta_0 - \theta_1)$ not plotted on nomogram (see text).

Figure 6. Mean sensible heating (S) between shore and downwind cloud free distance (x), local vertical air-sea temperature difference $(\theta_0 - \theta)$, and boundary layer height (Z_B) versus x for 20% relative humidity (RH) with θ_1 = 3°C (solid curves as marked).

Symbols correspond to other initial shore conditions as shown in legend. All for $(\theta_0 - \theta_1) = 11°C$, and $\Gamma_\theta = 3.8°C\ km^{-1}$.

Figure 7. Z_B-normalized correction factor for mean sensible heating $(\Delta S/S)/Z_B$ versus the initial potential temperature lapse rate (Γ_θ) for various land air-sea surface temperature differences $(\theta_0 - \theta_1)$. Z_B(km) is the boundary layer height at the downwind edge of the region in which S is computed.

Figure 8. Sames as Fig. 7, except for Z_B-normalized correction factor for mean latent heating, $(\Delta E/E)/Z_B$.

Figure 9. Slope of $Z_B{}^2$ versus the initial potential temperature lapse rate (Γ_θ) for various $(\theta_0 - \theta_1)$ under nondivergent conditions.

Figure 10. Cold air outbreak on 17 February 1979 as seen by Tiros-N AVHRR IR channel at 1941 GMT. Brightness temperatures are color coded according to color bar at bottom in steps of 1.8°C. Abscissa and ordinate are marked in longitude and latitude. Coastal waters in pink, red, and purple from Maine to Chesapeake Bay are in range of -1.5°C to 5.5°C. Northermost cloud edges appear stippled because clouds are broken. Cloud streets appear clearly in green south of Long Island and Connecticut, and in blue or green southeast of coast of Maine. Coldest cloud temperatures are green (-21°C) along 38° latitude.

Figure 11. Surface weather map of 17 February 1979 at 1500 GMT. Note snow at Cape Hatteras and winds at three buoys.

Figure 12. Weekly mean sea surface temperature for the period 14-21 February 1979.

Figure 13. Diurnal variations of cloud free path (circles) and the mean sensible heating between shore and cloud edge (solid curve and squares) for 17 February 1979 cold air out-

break off coastal area of Long Island, New York. Solid line is computed from the bulk transfer formula and the squares are estimated from the nomogram, both using data at shore and buoy.

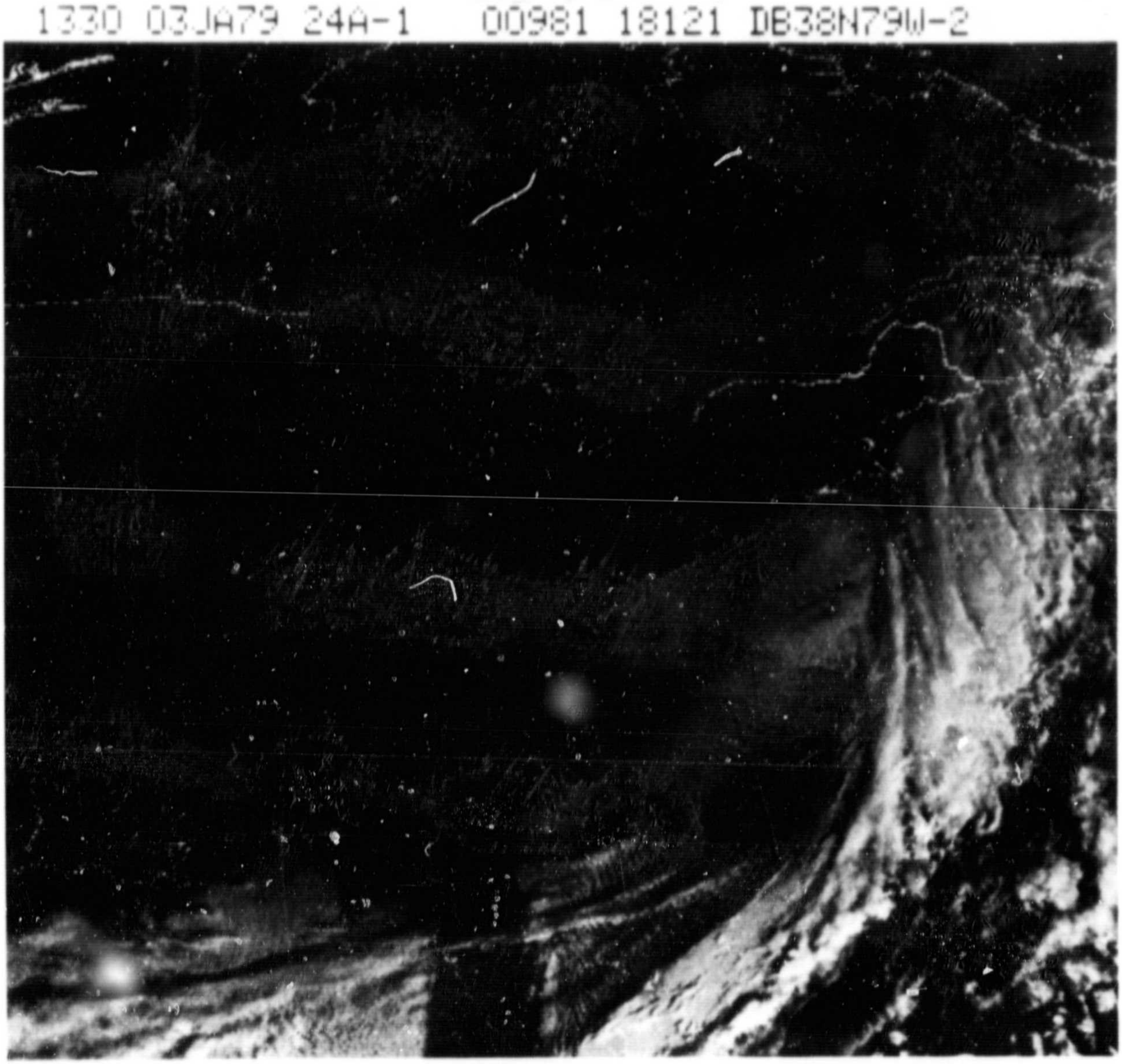

Figure 1. Cold air outbreak on 3 January 1979 as seen by GOES-2 visible channel. Note that shoreward edge of clouds is nearly an image of the coastline.

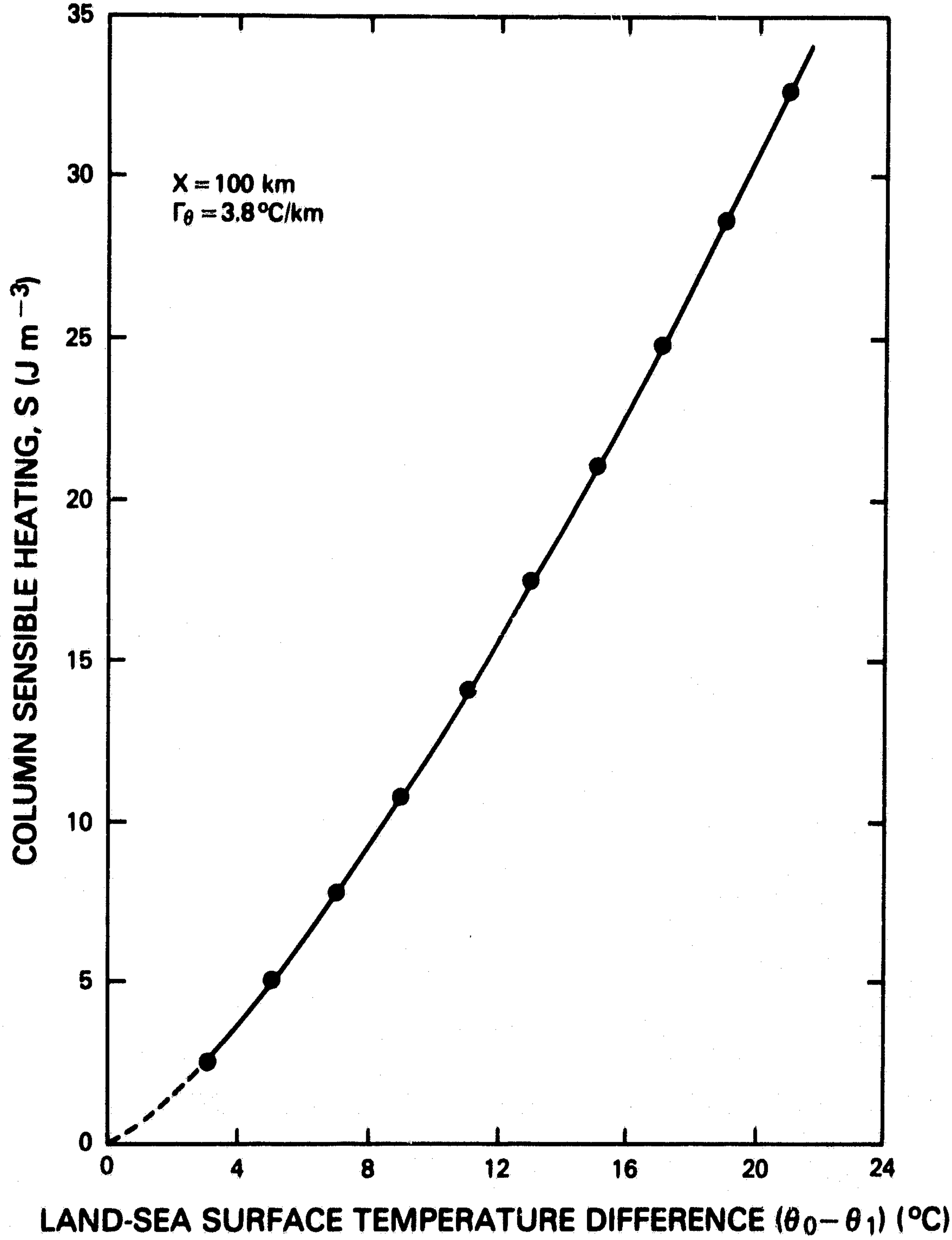

Figure 2. Mean column sensible heating (S) between shore and 100 km versus land air-sea surface temperature difference ($\theta_0 - \theta_1$) for an initial surface RH of 20% with θ_1 = 3°C and initial potential temperature lapse rate (Γ_θ) of 3.8°C km^{-1}.

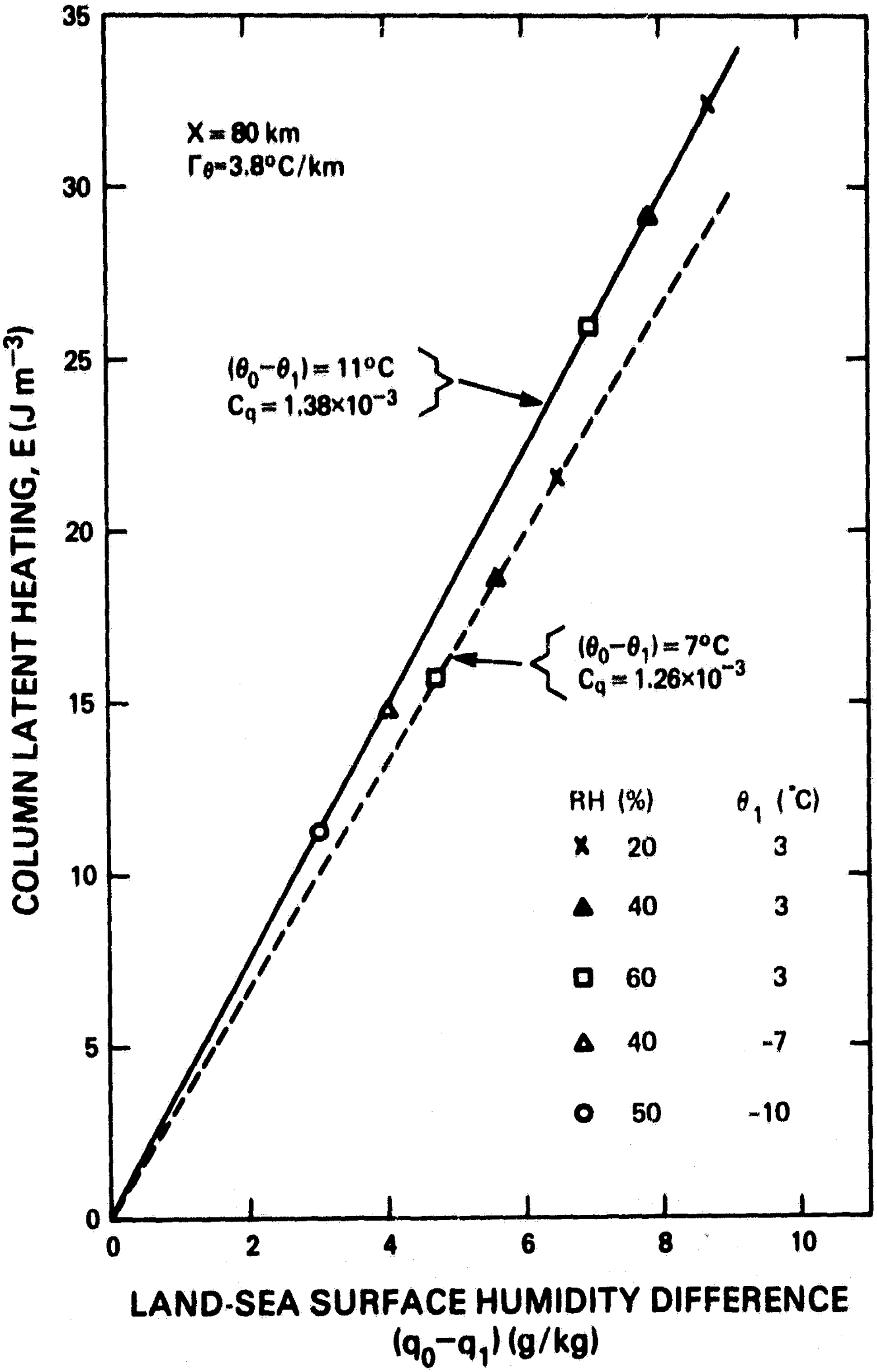

Figure 3. Mean column latent heating (E) between shore and 80 km versus land air-sea surface humidity difference $(q_0 - q_1)$. Solid line corresponds to $(\theta_0 - \theta_1) = 11°C$, and dashed line to $(\theta_0 - \theta_1) = 7°C$. All for the initial potential temperature lapse rate (Γ_θ) of 3.8°C km^{-1}. Symbols in legend correspond to various initial soundings.

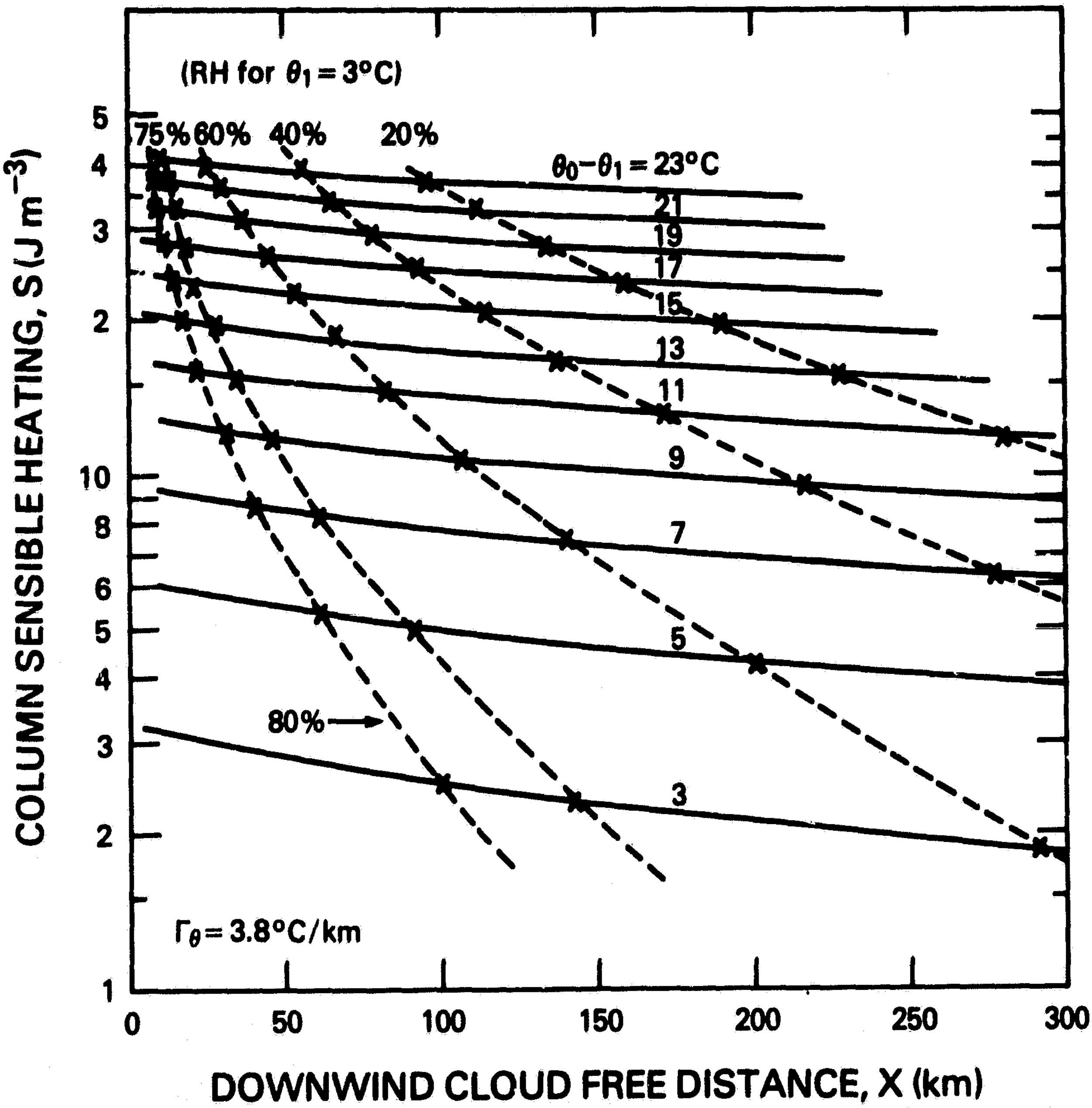

Figure 4. Mean column sensible heating (S) between shore and downwind cloud free distance (x) versus x for various land air-sea surface temperature differences ($\theta_0 - \theta_1$) under nondivergent conditions and initial potential temperature lapse rate of 3.8°C km^{-1} (solid lines). Dashed lines correspond to the cloud free paths for various surface relative humidities (RH) and initial shore surface air temperature (θ_1) of 3°C. Each cross indicates a numerical experiment.

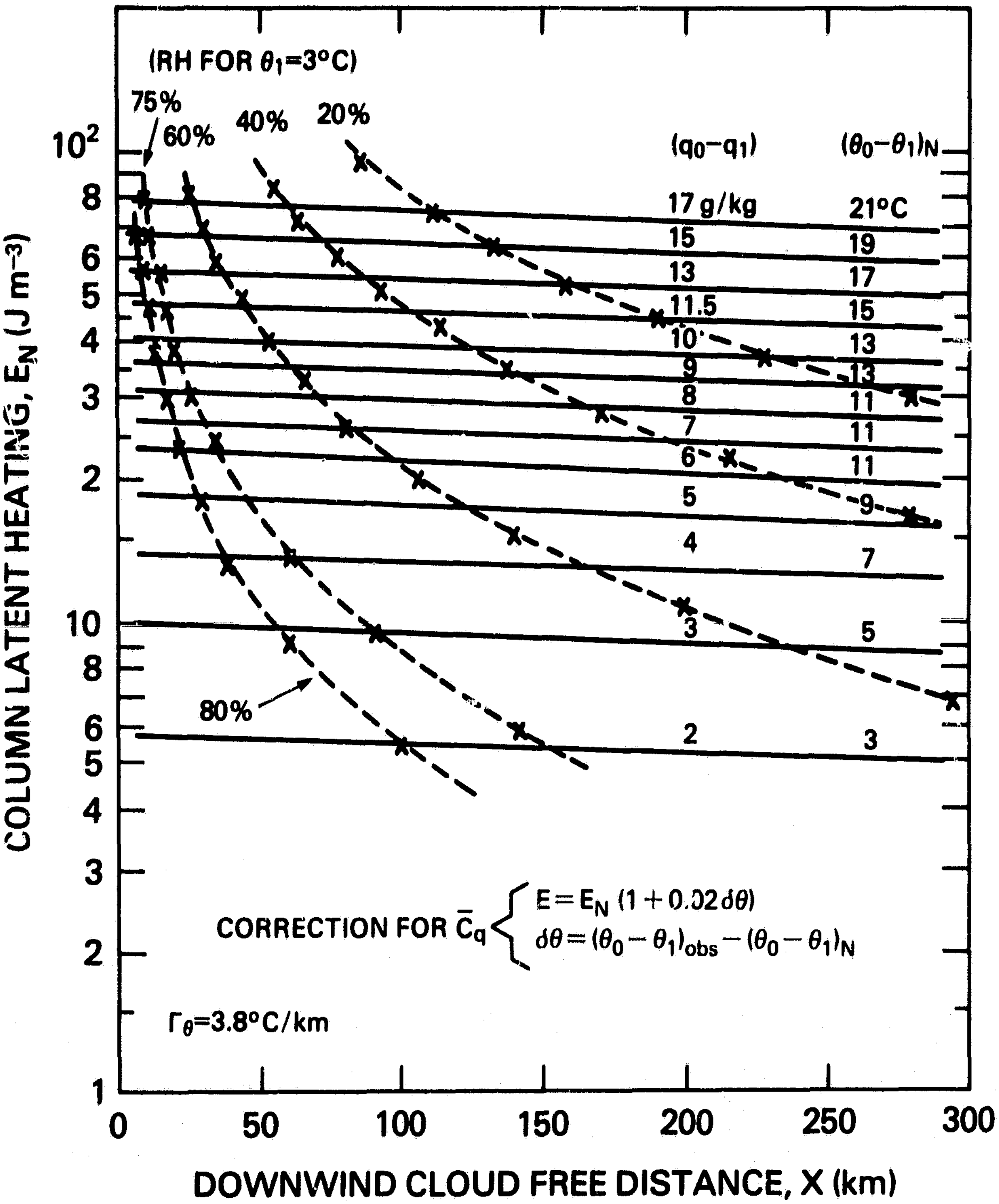

Figure 5. Same as Fig. 4, except for the dependence of mean column latent heating (E) on land air-sea surface humidity difference ($q_0 - q_1$) and land air-sea surface temperature difference ($\theta_0 - \theta_1$). Equation at bottom shows corrections in E due to values of ($\theta_0 - \theta_1$) not plotted on nomogram (see text).

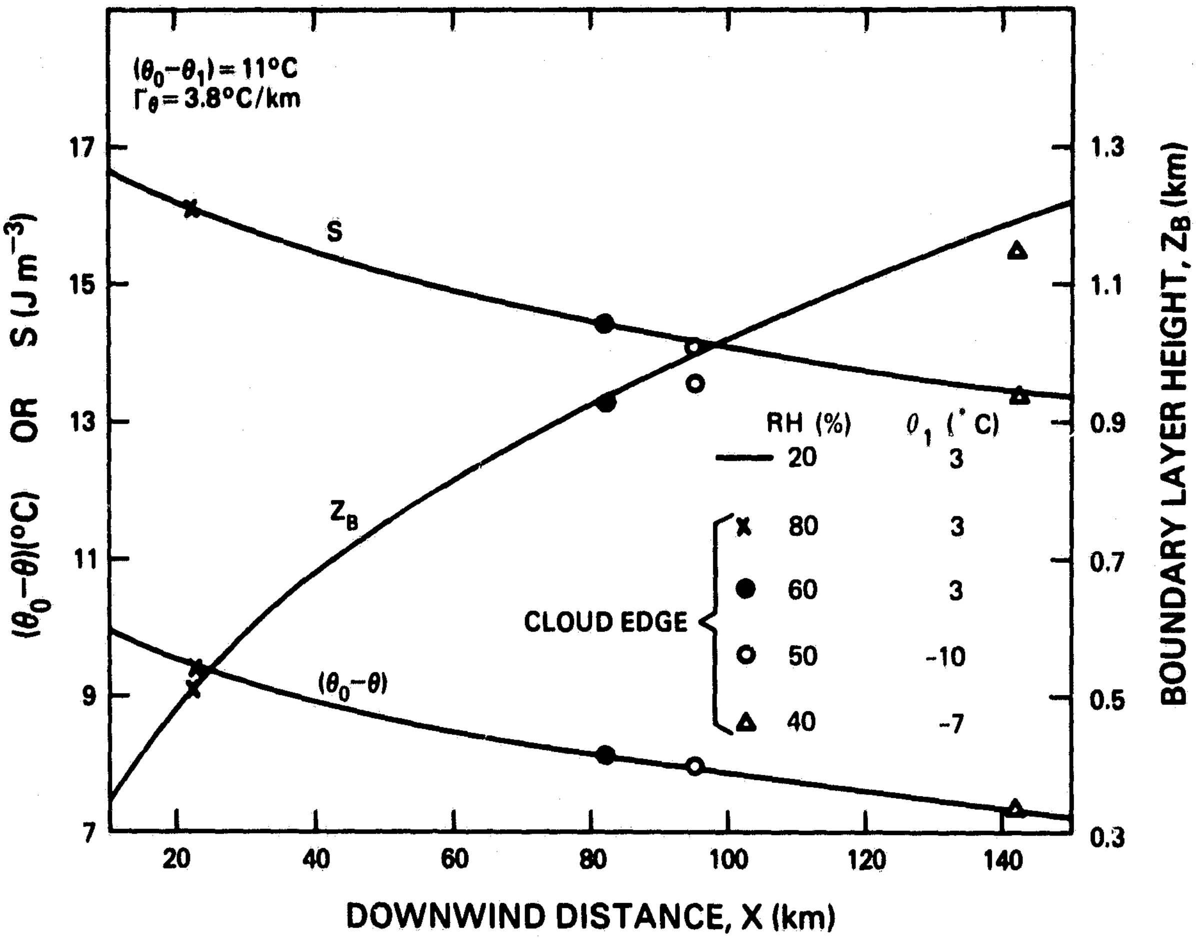

Figure 6. Mean sensible heating (S) between shore and downwind cloud free distance (x), local vertical air-sea temperature difference ($\theta_0 - \theta$), and boundary layer height (Z_B) versus x for 20% relative humidity (RH) with $\theta_1 = 3°C$ (solid curves as marked). Symbols correspond to other initial shore conditions as shown in legend. All for ($\theta_0 - \theta_1$) = 11°C, and Γ_θ = 3.8°C km^{-1}.

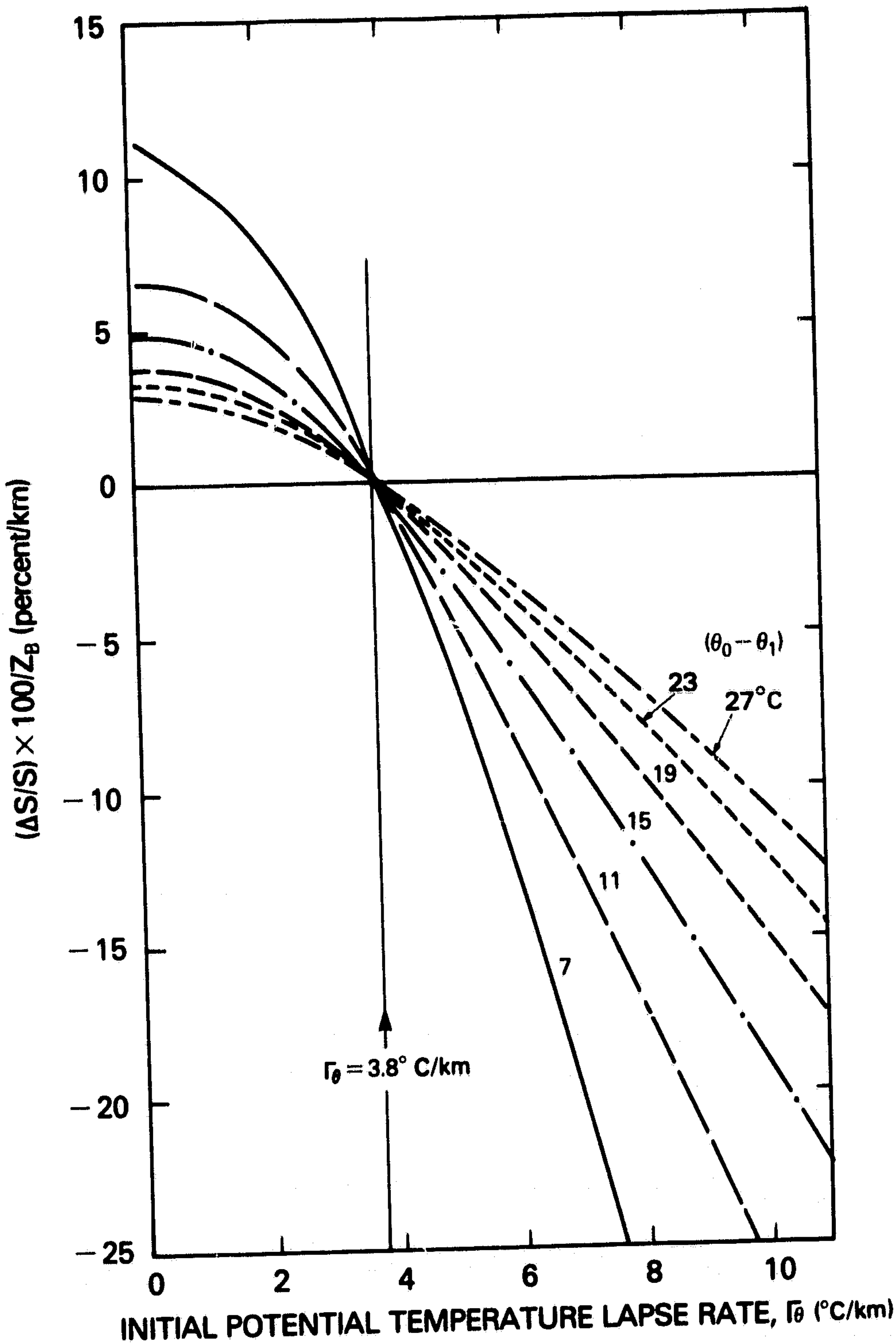

Figure 7. Z_B-normalized correction factor for mean sensible heating $(\Delta S/S)/Z_B$ versus the initial potential temperature lapse rate (Γ_θ) for various land air-sea surface temperature differences ($\theta_0 - \theta_1$). Z_B(km) is the boundary layer height at the downwind edge of the region in which S is computed.

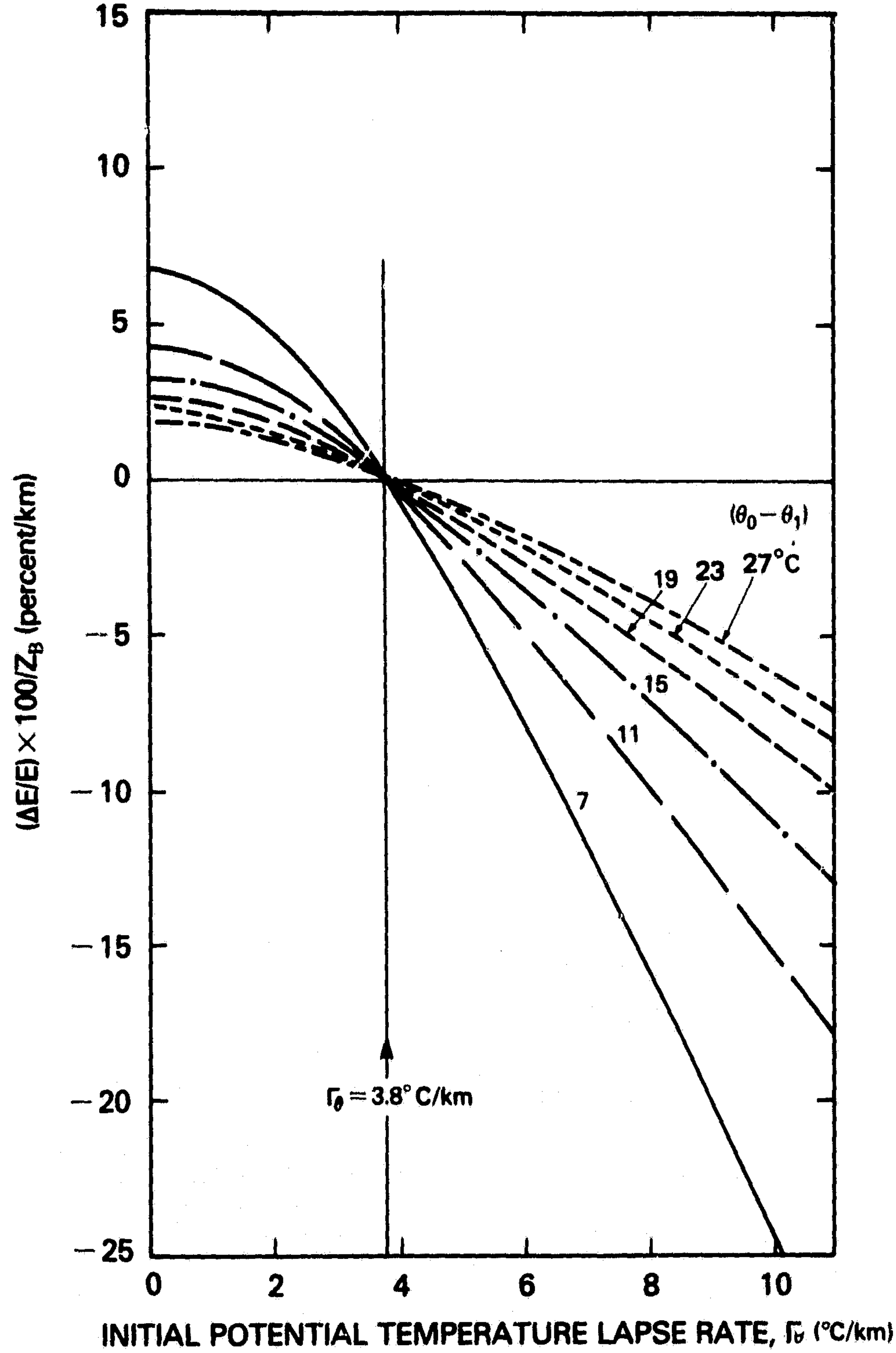

Figure 8. Same as Fig. 7, except for Z_B-normalized correction factor for mean latent heating, $(\Delta E/E)/Z_B$.

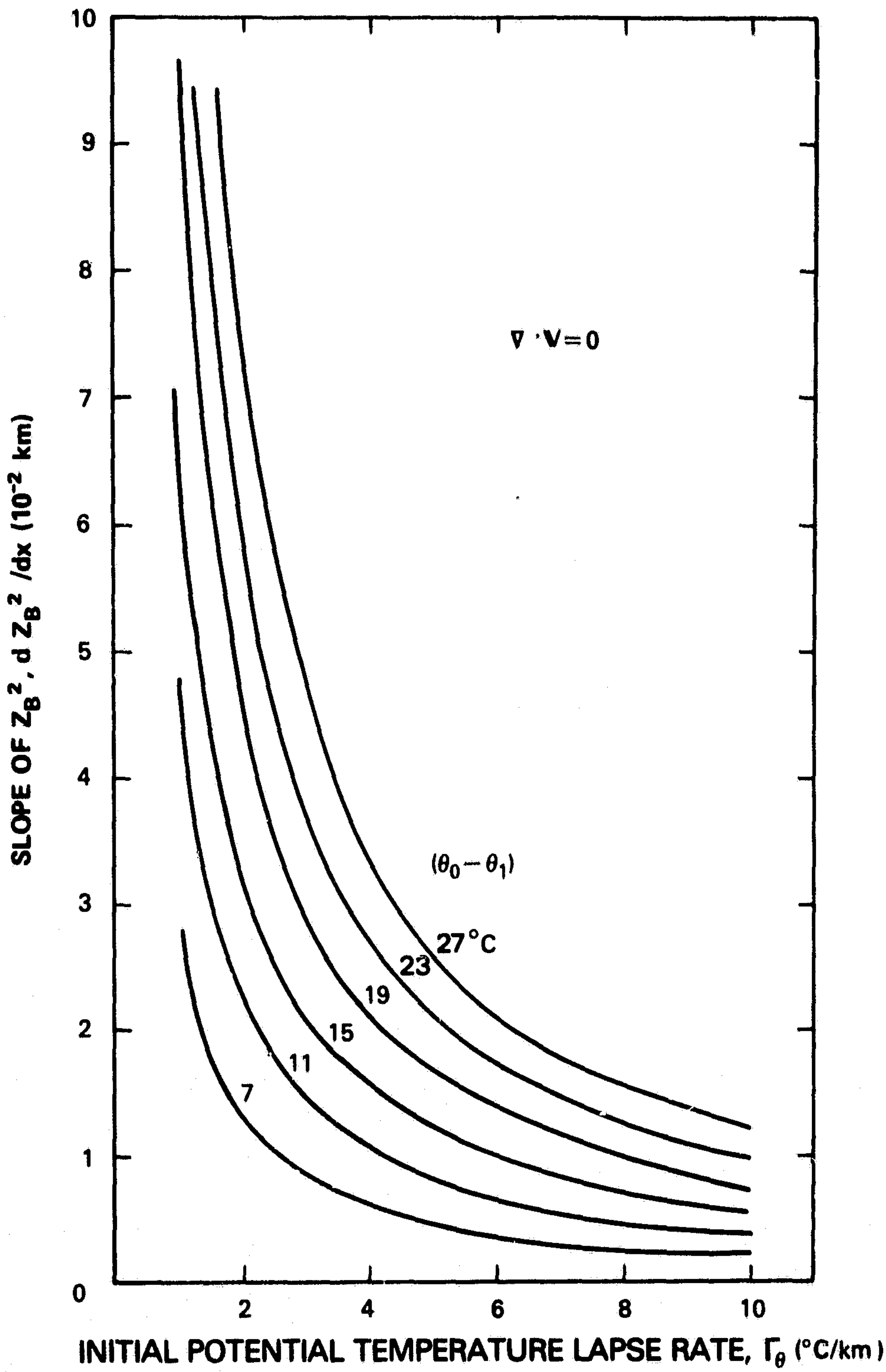

Figure 9. Slope of $Z_B{}^2$ versus the initial potential temperature lapse rate (Γ_θ) for various (θ_0 - θ_1) under nondivergent conditions.

Figure 10. Cold air outbreak on 17 February 1979 as seen by Tiros-N AVHRR IR channel at 1941 GMT. Brightness temperatures are color coded according to color [illegible] at bottom in steps of 1.8°C. Abscissa and ordinate are marked in longitude and latitude. Coastal waters in pink, red, and purple from Maine to Chesapeake Bay are in range of -1.5°C to 5.5°C. Northermost cloud edges appear stippled because clouds are broken. Cloud streets appear clearly in green south of Long Island and Connecticut, and in blue or green southeast of coast of Maine. Coldest cloud temperatures are green (-21°C) along 38° latitude.


0
100
200
500
1000
KILOMETERS

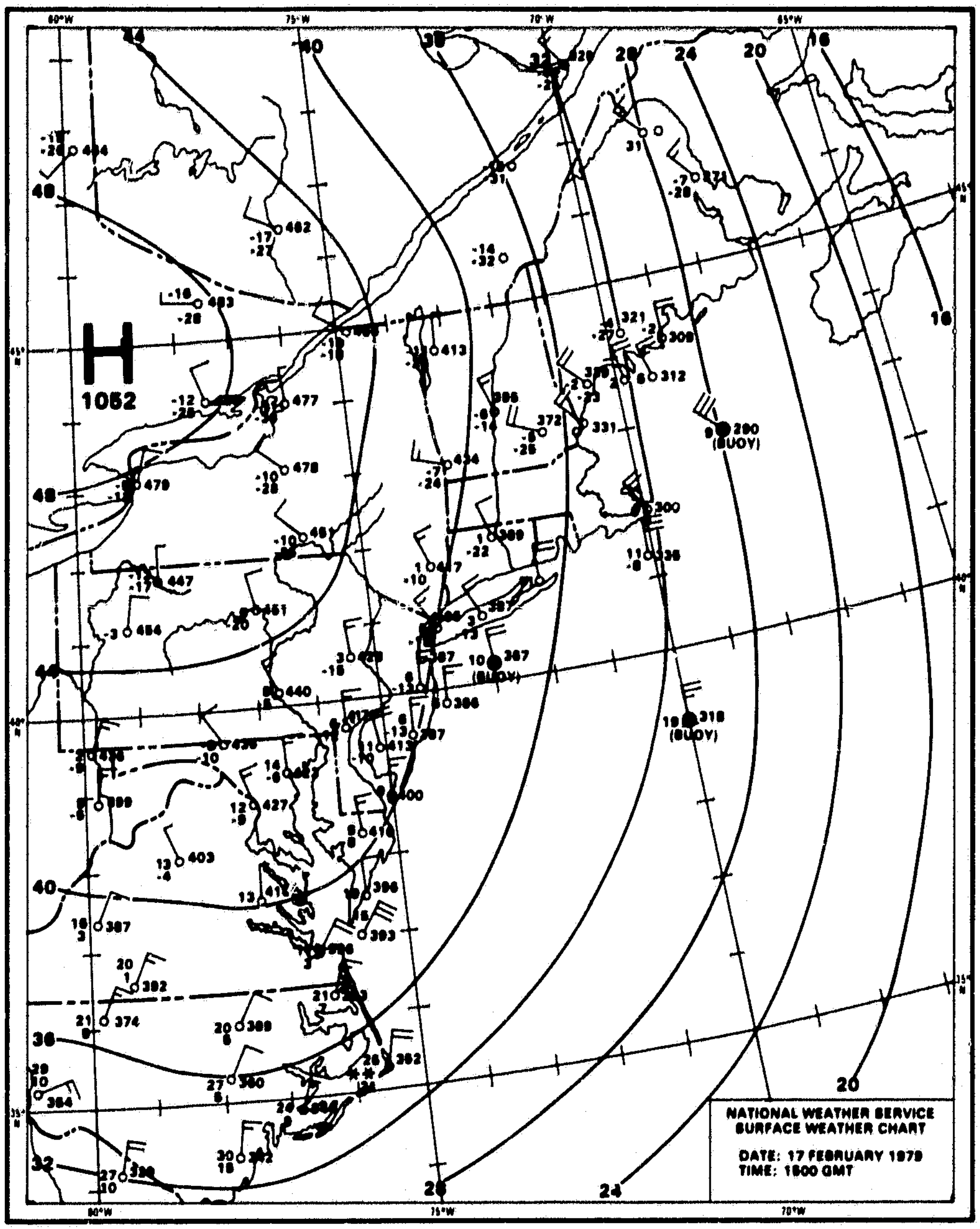

LATITUDE
U.S. EAST COAST

Figure 11. Surface weather map of 17 February 1979 at 1500 GMT. Note snow at Cape Hatteras and winds at three buoys.

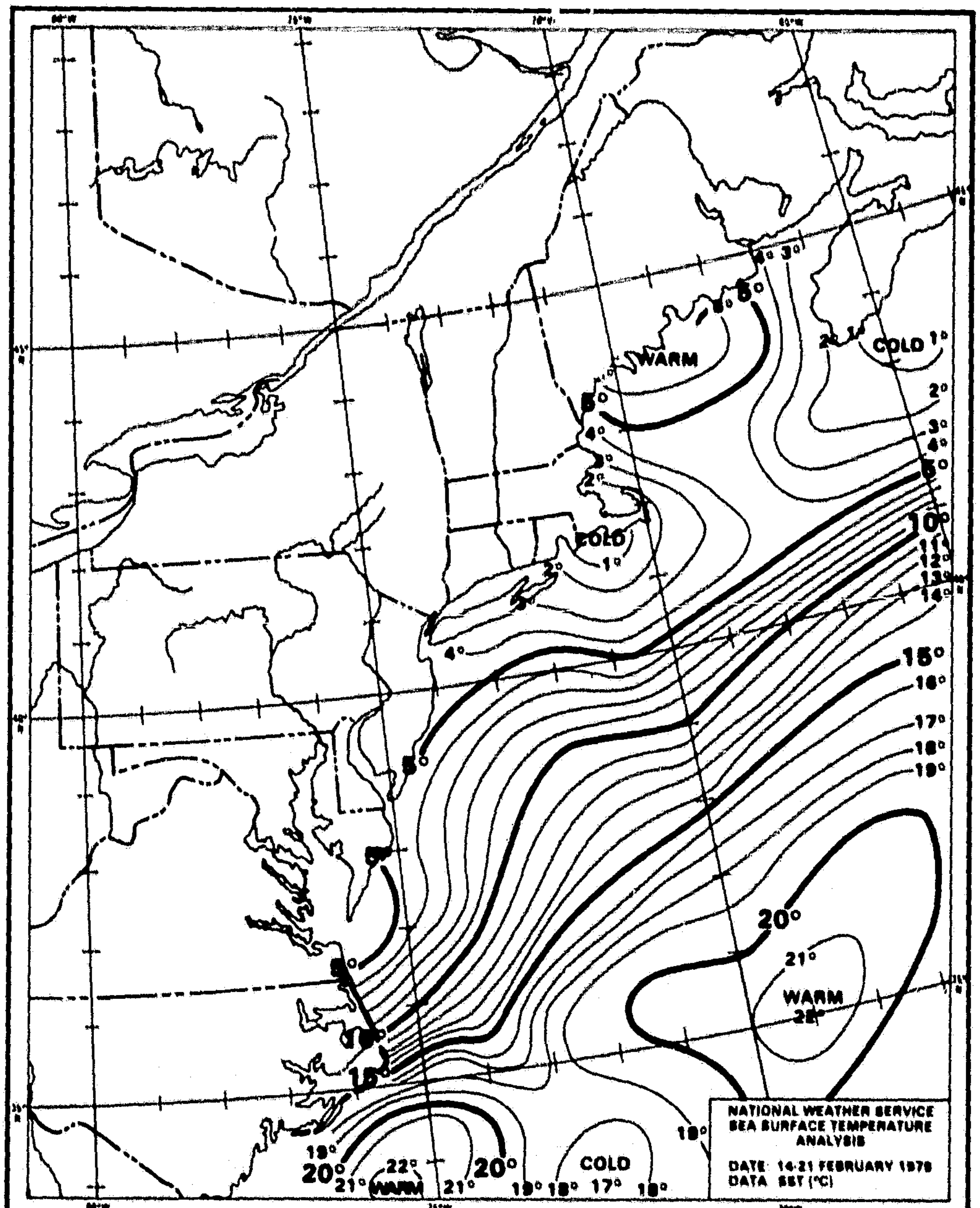

LATITUDE
U.S. EAST COAST

Figure 12. Weekly mean sea surface temperature for the period 14-21 February 1979.

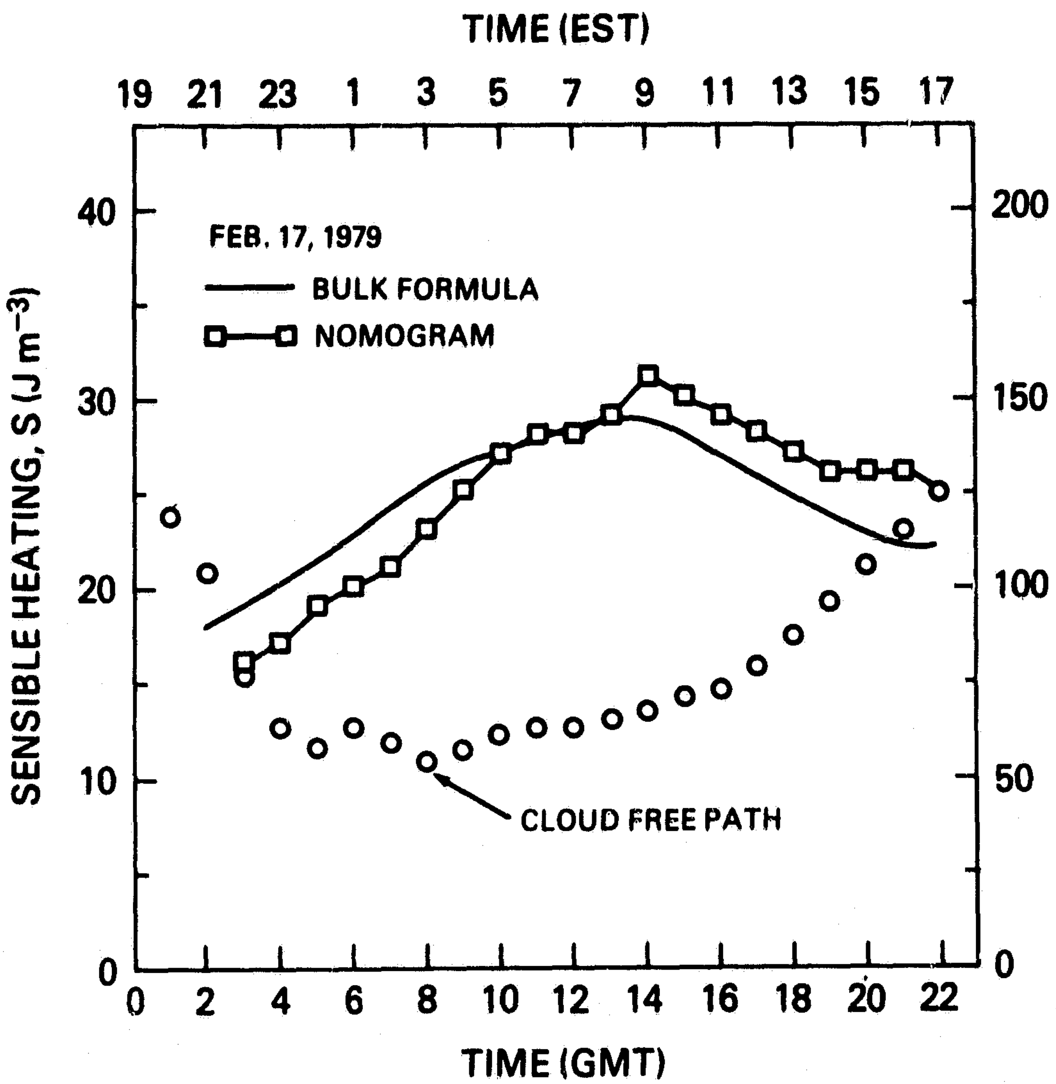

Figure 13. Diurnal variations of cloud free path (circles) and the mean sensible heating between shore and cloud edge (solid curve and squares) for 17 February 1979 cold air outbreak off coastal area of Long Island, New York. Solid line is computed from the bulk transfer formula and the squares are estimated from the nomogram, both using data at shore and buoy.